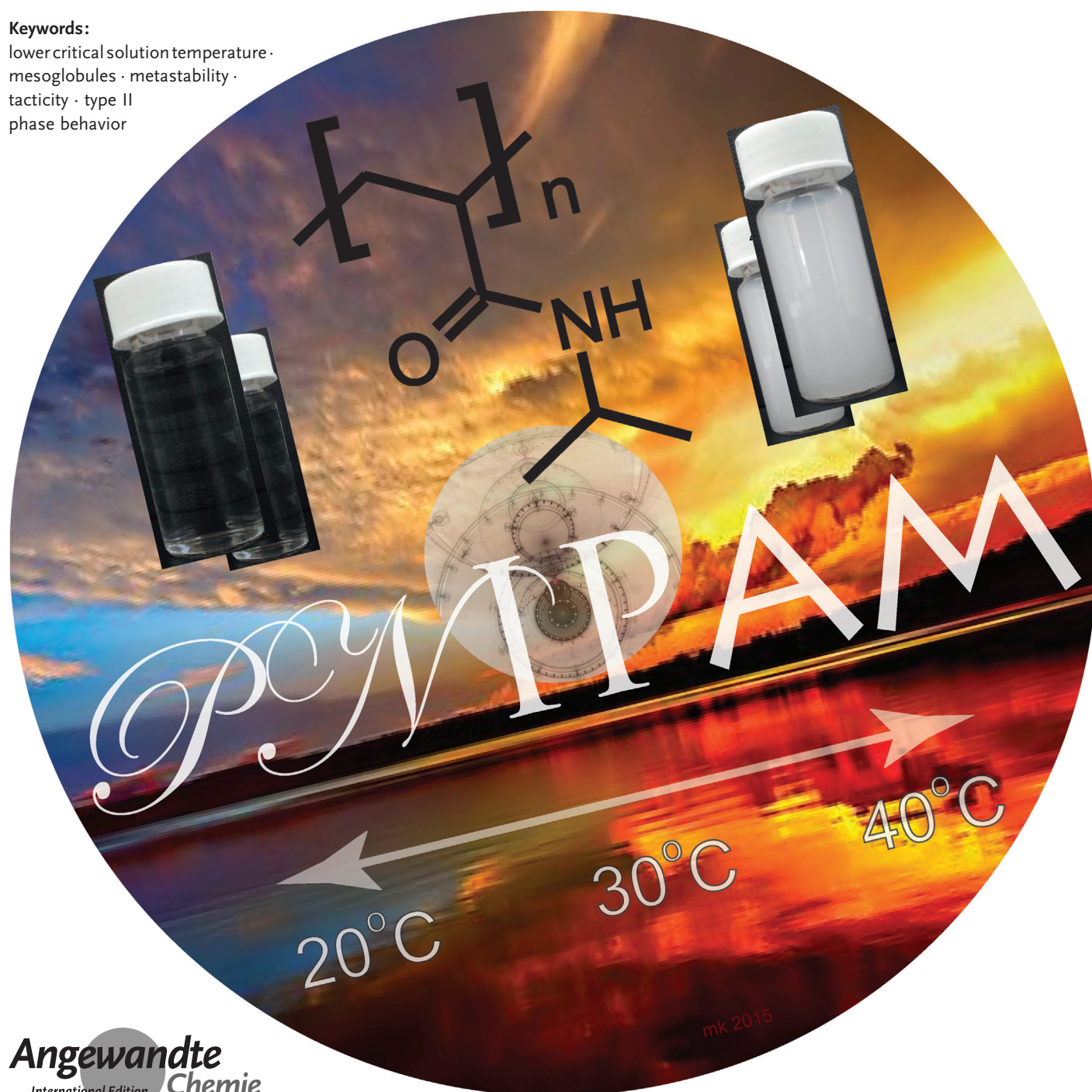


# Poly(*N*-isopropylacrylamide) Phase Diagrams: Fifty Years of Research

Avraham Halperin,\* Martin Kröger,\* and Françoise M. Winnik\*

**Keywords:**

lower critical solution temperature ·  
mesoglobules · metastability ·  
tacticity · type II  
phase behavior



In 1968, Heskins and Guillet published the first systematic study of the phase diagram of poly(*N*-isopropylacrylamide) (PNIPAM), at the time a “young polymer” first synthesized in 1956. Since then, PNIPAM became the leading member of the growing families of thermoresponsive polymers and of stimuli-responsive, “smart” polymers in general. Its thermal response is unanimously attributed to its phase behavior. Yet, in spite of 50 years of research, a coherent quantitative picture remains elusive. In this Review we survey the reported phase diagrams, discuss the differences and comment on theoretical ideas regarding their possible origins. We aim to alert the PNIPAM community to open questions in this reputedly mature domain.

## 1. Introduction

Poly(*N*-isopropylacrylamide) (PNIPAM) is the most commonly and successfully studied among thermoresponsive polymers.<sup>[1–4]</sup> Its thermal responsiveness is related to a miscibility gap observed in aqueous solutions above the lower critical solution temperature (LCST)  $T_{LCST}$ , i.e., solutions of free PNIPAM chains demix upon heating to a temperature  $T > T_{LCST}$ . The steeply reduced solubility upon heating is associated with a concomitant sharp configurational transition: dilute single chains, gels and brushes of terminally anchored chains undergo collapse with an abrupt reduction of their size. Applications can harness either the precipitation or the collapse. Thus, bioseparation of proteins conjugated with PNIPAM exploit demixing,<sup>[5]</sup> while harvesting cell sheets from surfaces displaying PNIPAM brushes utilizes the collapse transition.<sup>[6]</sup> The intense interest in PNIPAM arises because its LCST occurs at near physiological conditions thus rendering this neutral water soluble polymer suitable for biotechnological applications. The  $T_{LCST} \approx 32^\circ\text{C}$  value often cited in the literature is traceable to the 1968 article of Heskins and Guillet<sup>[7]</sup> where the LCST was identified at  $T_{LCST} \approx 31^\circ\text{C}$  and monomer volume fraction  $\phi_{LCST} \approx 0.16$ . This pioneering work is the first having investigated in detail the phase diagram of aqueous PNIPAM solutions and it remains widely cited today. However, subsequent work in this area (Table 1) did not lead to a consensus and the reported results differ strongly from the phase diagram of Heskins and Guillet (Figure 1). The difficulties encountered in mapping the phase boundaries of PNIPAM are of significance beyond the research domain concerned with this particular polymer. Similar issues are encountered in the study of other neutral, “LCST based” thermoresponsive polymers<sup>[8]</sup> whose phase diagrams remain to be investigated in detail. This last group includes in particular numerous copolymers of PNIPAM where the choice of the co-monomer, its fraction and its hydrophilicity/hydrophobicity serve to tune the thermal behavior.<sup>[9]</sup> In turn, the screening and design of such polymers rely on phase diagrams, in particular the  $T_{LCST}$ , as indicators of the onset of thermal response. This use illustrates the practical interest in the problem. The elucidation of PNIPAM phase diagrams is also of fundamental interest. First, because it is

## From the Contents

<b>1. Introduction</b>	15343
<b>2. Binodals, Cloud-Point and Demixing Curves: a Reminder</b>	15344
<b>3. Experimental Factors Contributing to Diversity</b>	15349
<b>4. Arrested Demixing and Hysteresis</b>	15353
<b>5. Macroscopic Phase Transition versus Arrested Demixing and Slow Coalescence</b>	15356
<b>6. Type I versus Type II Phase Separations and the Mixing Free Energy: A Reminder</b>	15358
<b>7. Evidence for Type II Phase Separation and PNIPAM Brushes</b>	15359
<b>8. Synthesis Overview</b>	15360
<b>9. Summary and Outlook</b>	15364

closely related to the determination of the parameters of the mixing free energy of PNIPAM. This in turn serves to relate the phase boundaries to solution properties such as osmotic

[\*] Prof. A. Halperin  
LIPHY, Université Grenoble Alpes  
38000 Grenoble (France)  
and  
LIPHY, CNRS, 38000 Grenoble (France)  
E-mail: avraham.halperin@ujf-grenoble.fr

Prof. M. Kröger  
Polymer Physics, Department of Materials, ETH Zurich  
Leopold-Ruzicka-Weg 4, 8093 Zurich (Switzerland)  
E-mail: mk@mat.ethz.ch  
Homepage: <http://complexfluids.ethz.ch>

Prof. F. M. Winnik  
Department of Chemistry, Université de Montréal  
CP 6128 Succursale Centre Ville, Montréal, QC H3C 3J7 (Canada)  
and  
WPI International Center for Materials Nanoarchitectonics (MANA)  
National Institute for Materials Science  
1-1 Namiki, Tsukuba, Ibaraki 305-0044 (Japan)  
and  
Laboratory of Polymer Chemistry, Department of Chemistry  
University of Helsinki  
P.O. Box 55, 00014 Helsinki (Finland)  
E-mail: francoise.winnik@umontreal.ca

Supporting information and ORCID(s) from the author(s) for this article are available on the WWW under <http://dx.doi.org/10.1002/anie.201506663>.

pressure or to gel swelling behavior. Second, because it confronts unresolved issues concerning the nature of the demixing and collapse transitions of PNIPAM. These are exemplified by observations of long-lived mesoscopic globules that fail to undergo macroscopic phase separation.

With these observations in mind this Review aims to provide a survey of the phase diagrams reported for PNIPAM chains in water, discuss the possible origins of the differences between various data sets, and suggest lines for future research. Data related to PNIPAM gels and PNIPAM brushes grafted to surfaces are not included: this Review is limited to the phase diagrams of the free PNIPAM chains/water systems. Our distinctive starting point is a graphical comparison (Figure 1) between the experimental results reported during the 1968–2015 period focusing on studies reporting demixing curves. The raw data was digitized thus enabling to replot selected data sets to bring out common features and differences. These experimental results were obtained using samples with range of molecular weights, MW, and polydispersities (Table 1). They differ also in the details of the synthesis and measurement procedures as well as in the range of PNIPAM weight fractions,  $w$ , investigated. The raw data depicted in the panels of Figure 1 corresponds to groups of samples of high MW ( $\gtrsim 50$  kDa) and low MW ( $\lesssim 50$  kDa)

studied at “low  $w$ ”, with  $0 < w \leq 0.15$ , and at “high  $w$ ” reaching an upper  $w > 0.15$ . This depiction was chosen because of practical considerations: it permits to distinguish between individual curves. The divide at  $M_w \approx 50$  kDa was motivated by experimental results, to be discussed later, indicating that end-effects are significant only below 50 kDa. The  $w$  divide was chosen for convenience noting however that high  $w$  data are necessary to distinguish the LCST. As Figure 1 demonstrates, the quantitative consensus regarding the phase diagram of PNIPAM is limited. The mismatch between the various data sets is significant even when the comparison is restricted to recent data on high MW samples: The demixing curves differ in slopes and the demixing temperatures at comparable  $w$  vary by up to 7 K. The differences can reach ca. 20 K when the comparison includes low MW curves or the phase diagram of Heskins and Guillet.<sup>[7]</sup>

The marked disagreements depicted in Figure 1 raise two questions we attempt to address in the following. First, what are the origins of the diversity of demixing curves? Second, why is this issue significant? With regard to the “origins” question it is helpful to distinguish between two directions. One concerns various “technical” experimental issues involving measurement techniques and the characteristics of the polymer sample. These are discussed in Sections 2 and 3 and include polydispersity, overheating, end-effects, tacticity etc. The second direction, discussed in Section 4, involves the nature of the PNIPAM demixing phase transition as manifested in the experimental evidence for long lived mesoscopic aggregates and the failure to reach macroscopic phase separation. With regard to the significance issue, we already commented on the practical aspect. From a fundamental perspective there is an interest in the nature of the PNIPAM phase transition and it is worthwhile to note two points: One concerns the issue of slow equilibration and long lived mesoglobules. This relates to fundamental questions regarding polymer collapse and aggregation as discussed in Section 5. The second point concerns the evidence that PNIPAM exhibits type II phase behavior with an “off zero” critical point at high MW. This last aspect, discussed in Sections 6 and 7, has qualitative implications on the structure of PNIPAM brushes. Sections 2–7 draw attention to issues traceable to synthesis: end-effects, branching, MW and polydispersity. Synthesis considerations also play a role in the discussion of future research directions. With these observations in mind we present in Section 8 an overview of PNIPAM synthesis focusing on aspects relevant to phase diagram studies. We conclude with a summary of the main conclusions and outlook for future research.



Avraham Halperin studied at Hebrew University of Jerusalem and obtained his PhD in Theoretical Chemistry in 1982. After post-doctoral fellowships at Exxon Research and Engineering Company and the Collège de France he was a visiting scientist at the Max Planck Institute für Polymerforschung, Laboratoire Léon Brillouin and the University of Santa Barbara. He joined the CNRS in 1994 and is now emeritus research director in the Laboratory for Interdisciplinary Physics (LIPHY), Grenoble.



Martin Kröger received his PhD and habilitation in Theoretical Physics at the Technical University Berlin. After post-doctoral employments at Hebrew University Jerusalem, Isaac Newton Institute Cambridge, UC Santa Barbara, RIAS Orchestra Berlin, Toyota Motors, and invited professorships in Strasbourg and Metz (France), he joined ETH Zurich (Switzerland) in 1997 where he now serves as Professor for Computational Polymer Physics. He acts as Editor-in-chief of Applied Rheology - international journal.



Françoise M. Winnik obtained her PhD from the University of Toronto. She worked as a research scientist in the Xerox Research Center of Canada, before joining McMaster University (Hamilton ON) in 1993 as an Associate Professor. Since 2000, she is a professor in the Université de Montréal. She is a Principal Investigator in the WPI Center for Materials Nanoarchitectonics, National Institute for Materials Science, Tsukuba, Japan and a Finnish Distinguished Professor of the University of Helsinki, Finland. She acts Editor-in-chief of Langmuir.

## 2. Binodals, Cloud-Point and Demixing Curves: a Reminder

Polydispersity and the temperature quench depth (Figure 2) are important factors affecting the observed demixing curves. A discussion of these factors is also important in order to address terminology issues. To this end recall that the starting point of a typical experiment

**Table 1:** An overview of the articles reporting the demixing curves cited and reproduced in this Review.

Year <sup>[Ref]</sup> Author <sup>[a]</sup>	$M_w$ <sup>[b]</sup> $M_n$	$M_w/M_n$ <sup>[c]</sup>	$T$ range $w$ range	Solvent <sup>[d]</sup> Initiator	Method <sup>[f]</sup> Heating (+) or Cooling (-) rate	Figs. (dataset)
1968 <sup>[7]</sup> Heskins	290 kDa 1000 kDa	3.44	31.1–58.7 °C 0.0067–0.641	(U) water APS-SBS	visual turbidity/ultracentrifuge + 0.05 K min <sup>-1</sup>	1,2,4,5
1989 <sup>[18]</sup> Fujishige	300 kDa – kDa	–	31.0–31.0 °C 0.0003–0.010	(F) benzene-acetone (?) AIBN	transmittance at 500 nm + 1 K min <sup>-1</sup>	1c,5d
1989 <sup>[101]</sup> Inomata	2300 kDa 1900 kDa	1.21	33.5 °C 0.044–0.073	– water potassium persulfate	DSC not specified	7
1990 <sup>[25]</sup> Otake	2100 kDa 44 kDa	48.0	31.0–32.8 °C 0.0037–0.059	– water potassium persulfate	DSC + 1 K min <sup>-1</sup>	1c,5b (DSC + 1 K)
1990 <sup>[25]</sup> Otake	2100 kDa 44 kDa	48.0	30.9–35.2 °C 0.0037–0.059	– water potassium persulfate	visual turbidity – 1 K min <sup>-1</sup>	1c,5b (turb – 1 K)
1990 <sup>[25]</sup> Otake	2100 kDa 44 kDa	48.0	30.7–33.1 °C 0.0037–0.074	– water potassium persulfate	visual turbidity + 1 K min <sup>-1</sup>	1c,5b (turb + 1 K)
1990 <sup>[25]</sup> Otake	2100 kDa 44 kDa	48.0	31.0–33.9 °C 0.0037–0.074	– water potassium persulfate	DSC – 1 K min <sup>-1</sup>	1c,5b (DSC – 1K)
1997 <sup>[16]</sup> Boutris	– kDa 9 kDa	–	31.0–38.9 °C 0.0087–0.213	(U) benzene AIBN	DSC + 5 K min <sup>-1</sup>	1d,5f (5 K)
1997 <sup>[16]</sup> Boutris	– kDa 9 kDa	–	31.5–40.8 °C 0.0223–0.179	(U) benzene AIBN	transmittance at 500 nm + 0.2 K min <sup>-1</sup>	1d,5f (0.2 K)
1997 <sup>[105]</sup> Zeng	101 kDa – kDa	–	31.9–33.1 °C 0.0047–0.179	– –	–	1a,5c
1998 <sup>[19]</sup> Zheng	2100 kDa 1296 kDa	1.61	32.9–32.9 °C 0.0148–0.092	– <i>tert</i> -butanol AIBN	transm. He-Ne laser (632.8 nm) + 0.033 K min <sup>-1</sup>	1b,5d
1998 <sup>[19]</sup> Zheng	1210 kDa 1000 kDa	1.21	32.5–32.7 °C 0.0271–0.115	– <i>tert</i> -butanol AIBN	transm. He-Ne laser (632.8 nm) + 0.033 K min <sup>-1</sup>	1b,5c
1998 <sup>[19]</sup> Zheng	390 kDa 293 kDa	1.33	32.2–32.5 °C 0.0270–0.118	– <i>tert</i> -butanol AIBN	transm. He-Ne laser (632.8 nm) + 0.033 K min <sup>-1</sup>	1b,5c
1998 <sup>[19]</sup> Zheng	180 kDa 130 kDa	1.38	31.9–32.2 °C 0.0311–0.127	– <i>tert</i> -butanol AIBN	transm. He-Ne laser (632.8 nm) + 0.033 K min <sup>-1</sup>	1b,5d
1999 <sup>[20]</sup> Tong	101 kDa 82 kDa	1.23	30.6–33.2 °C 0.0012–0.549	– <i>tert</i> -butanol AIBN	transm. He-Ne laser (632.8 nm?) + 0.033 K min <sup>-1</sup>	1a,5c
1999 <sup>[20]</sup> Tong	49 kDa 41 kDa	1.21	30.2–32.5 °C 0.0118–0.699	– <i>tert</i> -butanol AIBN	transm. He-Ne laser (632.8 nm?) + 0.033 K min <sup>-1</sup>	1a,5c
2000 <sup>[29]</sup> Afroze	124 kDa 83 kDa	1.48	26.8–31.7 °C 0.0024–0.757	– toluene AIBN	DSC + 1 K min <sup>-1</sup>	1a,5a
2000 <sup>[29]</sup> Afroze	53 kDa 36 kDa	1.47	26.6–31.7 °C 0.0529–0.757	– toluene AIBN	DSC + 1 K min <sup>-1</sup>	1a,5a
2000 <sup>[29]</sup> Afroze	10 kDa 2 kDa	4.54	27.2–34.0 °C 0.0240–0.504	– THF AIBN	scattered light at 30° + 1 K min <sup>-1</sup>	1d,5a (turb)
2000 <sup>[29]</sup> Afroze	10 kDa 2 kDa	4.54	27.4–33.1 °C 0.0097–0.701	– THF AIBN	DSC + 1 K min <sup>-1</sup>	1d,5a (DSC)
2001 <sup>[26]</sup> G. de Azevedo	615 kDa 301 kDa	2.04	32.6–34.1 °C 0.0103–0.176	– water APS-SMBS	transm./sc. light of He-Ne I not specified	1a,5c

Table 1: (Continued)

Year <sup>[Ref]</sup> Author <sup>[a]</sup>	$M_w$ <sup>[b]</sup> $M_n$	$M_w/M_n$ <sup>[c]</sup>	$T$ range $\omega$ range		Solvent <sup>[d]</sup> Initiator	Method <sup>[f]</sup> Heating (+) or Cooling (–) rate	Figs. (dataset)
2003 <sup>[106]</sup> Milewska	525 kDa 260 kDa	2.01	32.9–33.5 °C 0.0171–0.109	–	water APS-SMBS	transm./sc. light of He-Ne I not specified	1b,5c
2004 <sup>[22]</sup> Van Durme	187 kDa 72 kDa	2.61	23.9–34.6 °C 0.0971–0.699	–	1,4-dioxane AIBN	transm. at 615 nm/mod. DSC + 1 K min <sup>–1</sup>	1a,5a
2004 <sup>[22]</sup> Van Durme	74 kDa 25 kDa	2.99	23.9–31.5 °C 0.0017–0.802	–	1,4-dioxane AIBN	transm. at 615 nm/mod. DSC + 1 K min <sup>–1</sup>	1a,5a (0.1 J g <sup>–1</sup> K <sup>–1</sup> )
2004 <sup>[22]</sup> Van Durme	74 kDa 25 kDa	2.99	23.9–31.5 °C 0.0500–0.798	–	1,4-dioxane AIBN	transm. at 615 nm/mod. DSC + 1 K min <sup>–1</sup>	1a,5a (1 J g <sup>–1</sup> K <sup>–1</sup> )
2004 <sup>[22]</sup> Van Durme	18 kDa 5 kDa	4.00	24.0–34.6 °C 0.0460–0.699	–	1,4-dioxane AIBN	transm. at 615 nm/mod. DSC + 1 K min <sup>–1</sup>	1d,5a
2006 <sup>[41]</sup> Furyk	475 kDa 360 kDa	1.32	30.1–30.3 °C 0.0020–0.050	(F)	methanol AIBN	microfluidic device with $T$ gradient –	1b,5d
2006 <sup>[41]</sup> Furyk	350 kDa – kDa	–	30.0–30.2 °C 0.0098–0.100	(F)	methanol AIBN	microfluidic device with $T$ gradient –	1b,5d
2006 <sup>[41]</sup> Furyk	56 kDa 31 kDa	1.81	29.9–31.0 °C 0.0021–0.050	(F)	methanol AIBN	microfluidic device with $T$ gradient –	1b,5c
2006 <sup>[23]</sup> Xia	58 kDa 29 kDa	2.00	31.5–36.1 °C 0.0010–0.080	–	methyl ethyl ketone AIBN	transmittance at 500 nm + 0.5 K min <sup>–1</sup>	1c,5b
2006 <sup>[23]</sup> Xia	22 kDa 19 kDa	1.11	29.2–33.7 °C 0.0010–0.080	–	2-propanol <i>N</i> -isopropyl-2-CPIA <sup>[e]</sup>	transmittance at 500 nm + 0.5 K min <sup>–1</sup>	1e,5b
2008 <sup>[34]</sup> Katsumoto	44 kDa 34 kDa	1.29	23.5–25.2 °C 0.009–0.080	–	– AIBN	transmittance at 650 nm –	4 (64%)
2008 <sup>[34]</sup> Katsumoto	39 kDa 30 kDa	1.30	25.0–26.0 °C 0.009–0.080	–	– AIBN	transmittance at 650 nm –	4 (60%)
2008 <sup>[34]</sup> Katsumoto	36 kDa 32 kDa	1.11	28.7–32.7 °C 0.009–0.080	–	– AIBN	transmittance at 650 nm –	4 (46%)
2008 <sup>[17]</sup> Kawaguchi	144 kDa 126 kDa	1.14	30.7–31.5 °C 0.0047–0.095	(F)	benzene AIBN	transmittance at 650 nm + 0.025 K min <sup>–1</sup>	1b,5c
2008 <sup>[17]</sup> Kawaguchi	131 kDa 107 kDa	1.23	31.8–32.5 °C 0.0052–0.085	(F)	<i>tert</i> -butanol AIBN	transmittance at 650 nm + 0.025 K min <sup>–1</sup>	1b,5c
2008 <sup>[17]</sup> Kawaguchi	127 kDa 108 kDa	1.18	30.6–31.6 °C 0.0058–0.092	(F)	1,4-dioxane AIBN	transmittance at 650 nm + 0.025 K min <sup>–1</sup>	1b,5c
2008 <sup>[17]</sup> Kawaguchi	94 kDa 81 kDa	1.16	32.1–32.8 °C 0.0051–0.086	(F)	methanol AIBN	transmittance at 650 nm + 0.025 K min <sup>–1</sup>	1b,5c
2008 <sup>[17]</sup> Kawaguchi	65 kDa 54 kDa	1.19	32.0–32.9 °C 0.0049–0.090	(F)	methanol AIBN	transmittance at 650 nm + 0.025 K min <sup>–1</sup>	1b,5c
2008 <sup>[17]</sup> Kawaguchi	52 kDa 45 kDa	1.13	31.4–32.7 °C 0.0050–0.095	(F)	<i>tert</i> -butanol AIBN	transmittance at 650 nm + 0.025 K min <sup>–1</sup>	1b,5c (t-b)
2008 <sup>[17]</sup> Kawaguchi	52 kDa 41 kDa	1.27	30.1–31.7 °C 0.0049–0.093	(F)	1,4-dioxane AIBN	transmittance at 650 nm + 0.025 K min <sup>–1</sup>	1b,5c (1,4-d)
2008 <sup>[17]</sup> Kawaguchi	47 kDa 40 kDa	1.17	30.4–31.6 °C 0.0050–0.097	(F)	benzene AIBN	transmittance at 650 nm + 0.025 K min <sup>–1</sup>	1b,5c

**Table 1:** (Continued)

Year <sup>[Ref]</sup> Author <sup>[a]</sup>	$M_w$ <sup>[b]</sup> $M_n$	$M_w/M_n$ <sup>[c]</sup>	$T$ range $w$ range	Solvent <sup>[d]</sup> Initiator	Method <sup>[f]</sup> Heating (+) or Cooling (-) rate	Figs. (dataset)
2008 <sup>[24]</sup> Zhou	390 kDa 355 kDa	1.09	28.3–31.2 °C 0.0485–0.595	(F) benzene AIBN	microfluidics/evaporation (3 runs) + 0.5 K min <sup>-1</sup>	1a,5a (i-iii)
2009 <sup>[28]</sup> Pamies	13 kDa 12 kDa	1.11	27.5–37.0 °C 0.0003–0.050	(F) water/DMF 50:50 ECP <sup>[e]</sup>	scattered light 654 nm + 0.2 K min <sup>-1</sup>	1e,5f
2009 <sup>[28]</sup> Pamies	9 kDa 8 kDa	1.12	27.5–38.5 °C 0.0003–0.050	(F) water/DMF 50:50 ECP <sup>[e]</sup>	scattered light 654 nm + 0.2 K min <sup>-1</sup>	1e,5f
2009 <sup>[28]</sup> Pamies	5 kDa 5 kDa	1.14	27.5–44.0 °C 0.0003–0.050	(F) water/DMF 50:50 ECP <sup>[e]</sup>	scattered light 654 nm + 0.2 K min <sup>-1</sup>	1e,5f
2011 <sup>[36]</sup> Nakano	306 kDa 106 kDa	2.90	24.0–28.5 °C 0.0009–0.060	– –	– –	4 (64%)
2011 <sup>[36]</sup> Nakano	270 kDa 73 kDa	3.69	32.0–33.6 °C 0.0002–0.060	– –	– –	4 (64%)
2011 <sup>[107]</sup> Poschlad	104 kDa 74 kDa	1.41	33.4–35.9 °C 0.00002–0.04	– water THF	– visual turbidity + 0.02 K min <sup>-1</sup>	1b (turb)
2011 <sup>[107]</sup> Poschlad	104 kDa 74 kDa	1.41	33.4–35.9 °C 0.0003–0.08	– water THF	– refractometry + 0.033 K min <sup>-1</sup>	1b (ri)
2011 <sup>[30]</sup> Shi	478 kDa 435 kDa	1.10	31.8–33.4 °C 0.0055–0.087	– benzene AIBN	– microfluidics, droplets of different concentration	1c,5b (mf)
2011 <sup>[30]</sup> Shi	478 kDa 435 kDa	1.10	33.0–34.1 °C 0.0171–0.086	– benzene AIBN	– scattered light at 90° –	1c,5b (ls)
2013 <sup>[108]</sup> Hashimoto	1090 kDa – kDa	–	31.8–33.9 °C 0.0004–0.148	– methanol AIBN	– scattering at 448 nm at 90° + 0.033 K min <sup>-1</sup>	1a,5a
2014 <sup>[31]</sup> Philipp	23 kDa – kDa	–	32.0–34.4 °C 0.0062–0.301	– –	– refractometry + 0.5 K min <sup>-1</sup>	1d,5a

[a] The entries are labeled by year of publication and first author. [b] Weight-averaged molecular mass,  $M_w$ , and number-averaged molecular mass,  $M_n$ . [c] PDI. [d] Solvent and initiator used for the polymerization reaction. Unless otherwise indicated, the synthesis utilizes conventional free radical polymerization (Scheme 1). [e] Synthesis by atom-transfer radical polymerization (ATRP, Scheme 3). [f] Method utilized to characterize the onset of demixing. AIBN = 2,2'-azobis(isobutyronitrile), (U) = unfractionated, (F) = fractionated, ECP = ethyl 2-chloropropionate, APS = ammonium persulfate, CPIA = chloropropionamide, SBS = sodium bisulfite, SMBS = sodium metabisulfite.

exploring the phase diagram is a polydisperse, dry PNIPAM sample. The sample composition is characterized by its weight averaged molecular mass,  $M_w$ , and its number averaged molecular mass,  $M_n$ , or polydispersity index (PDI)  $M_w/M_n$ . These provide partial information regarding the distribution of chain lengths. This initial sample is used to prepare a series of solutions of different overall polymer weight fractions  $w$  yet having identical distribution of polymerization degrees  $N$ . Such solutions are known as quasibinary and their full phase diagram is described in a  $k$ -dimensional space defined by the temperature  $T$  and the  $k-1$  axes specifying the weight fraction of each component of the polydisperse solution. The solutions are then heated gradually and the onset of demixing is identified by an upturn of turbidity, the endotherm of differential scanning calorimetry (DSC) etc. Each demixing temperature  $T_{\text{dem}}$  corresponds to a specific  $w$ , and the  $T_{\text{dem}}(w)$  curve is often referred to as cloud point curve. This term acquired however two somewhat different meanings. One

definition is encountered in the theory of phase diagrams and refers to a state of thermodynamic equilibrium.<sup>[10–12]</sup> Within this convention each point on the cloud point curve corresponds to the intersection of two curves: i) the composition curve describing the sequential dilutions of a given sample thus having identical  $N$  distribution and ii) the coexistence curve of the polydisperse solution.<sup>[10,11]</sup> In another convention, the cloud point curve denotes the experimentally obtained  $T_{\text{dem}}(w)$  demixing curve which also reflects non-equilibrium effects such as overheating.<sup>[13]</sup> To avoid confusion we will utilize the term demixing curve when referring to the second, experimental situation.

Altogether it is thus necessary to distinguish between three curves: i) The binodal or coexistence curve of the polydisperse solution, ii) the cloud point curve defined by the intersection between the binodal and the composition curve specified by the particular chain length distribution of the sample, and iii) the experimentally observed demixing curve.

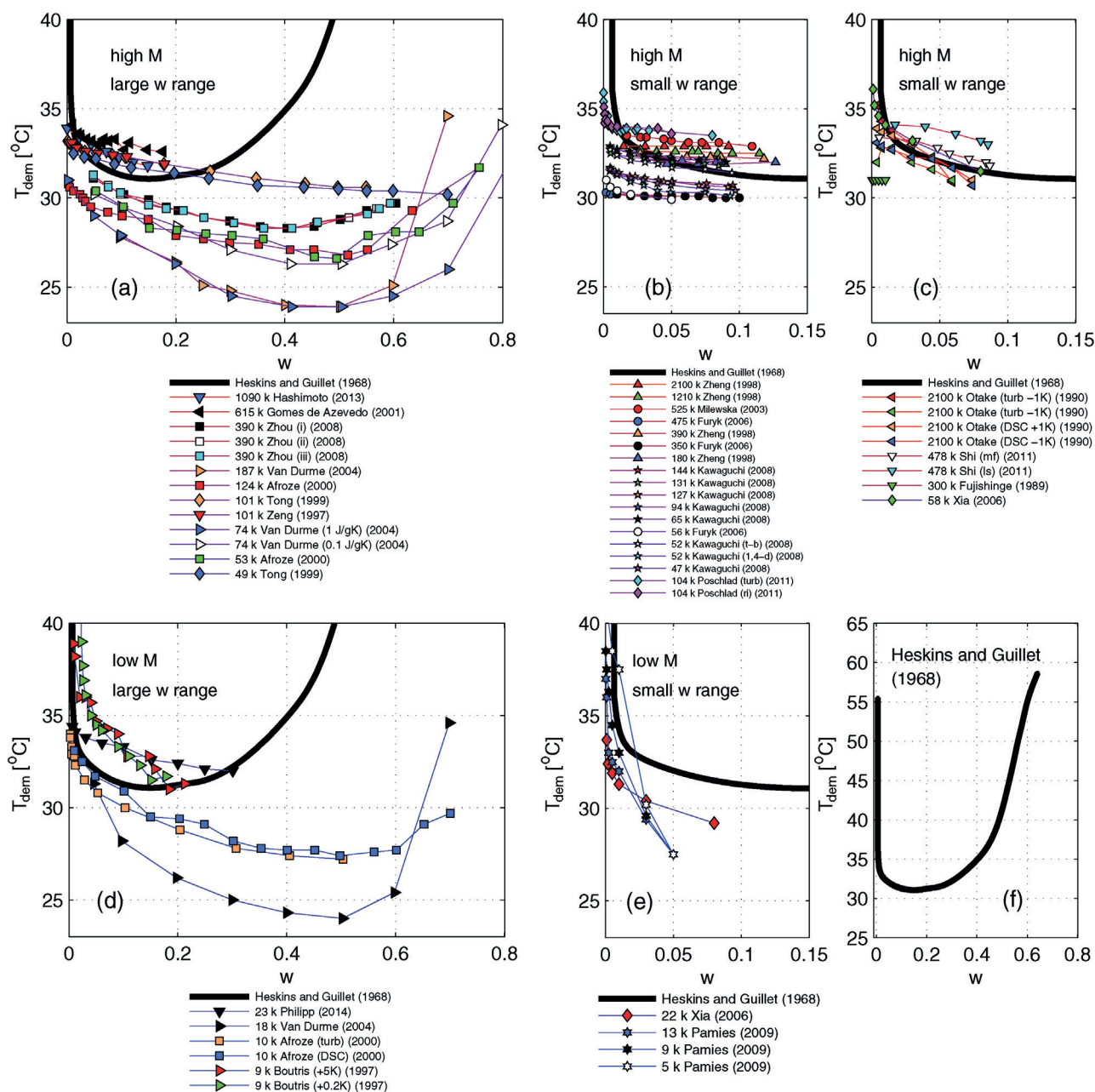
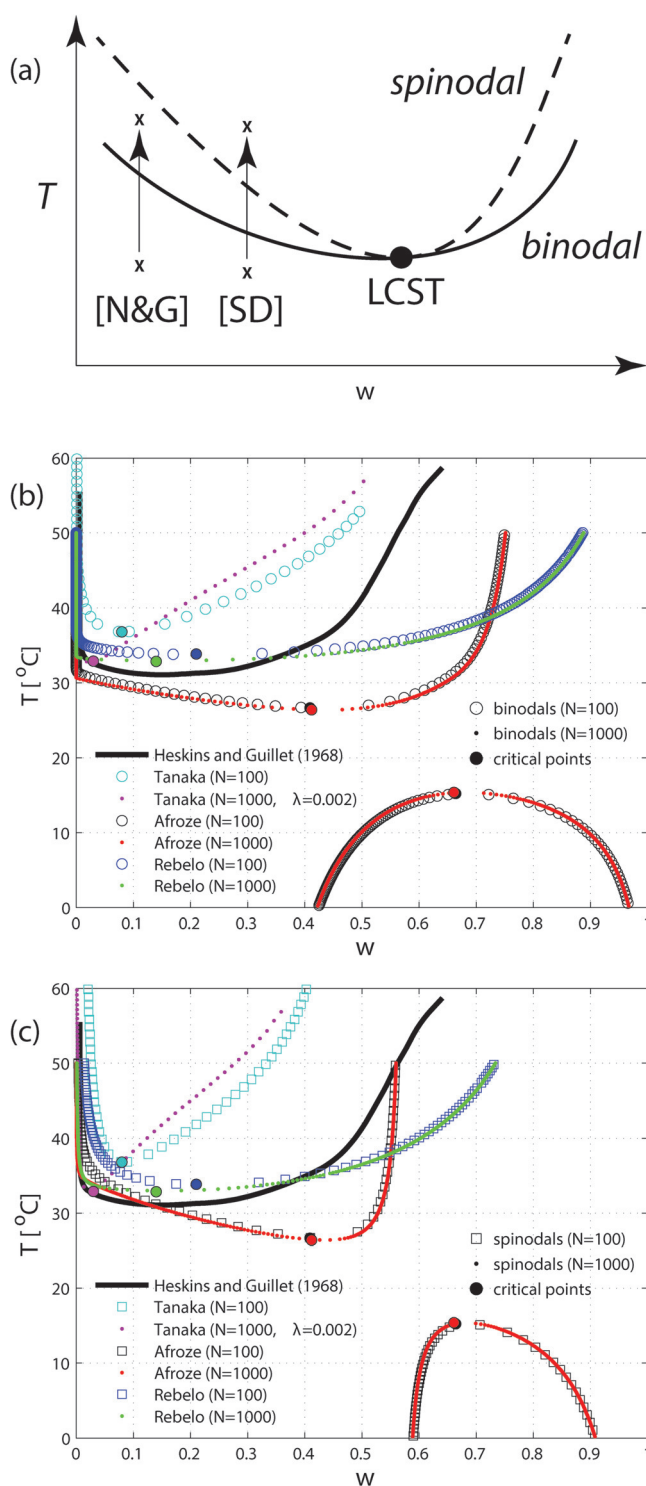


**Figure 1.** The temperature  $T_{\text{dem}}$  vs. weight fraction  $w$  demixing curves as reported in the articles listed in Table 1. To distinguish between different curves the data sets were grouped into five panels, (a–e), according to molecular mass,  $w$  range and the slope of the phase boundary at intermediate  $w$ . To facilitate comparison, the panels have an identical  $T$  axis and incorporate, as a reference, the relevant portion of the Heskins and Guillet demixing curve<sup>[7]</sup> depicted in full in panel (f). The legends of the panels are labeled by MW, first author and year of publication. When this information is insufficient the label is extended to include details of synthesis or measurement: laser light scattering (ls), microfluidic device (mf), calorimetric measurements (DSC), optical measurements (opt), potassium persulfate (pp), tert-butyl alcohol (tb), 1,4-dioxane (1,4-d), heating at a rate of  $x\text{K min}^{-1}$  (+xK), cooling at a rate of  $x\text{K min}^{-1}$  (–xK), first and second measurement (i,ii), as in Table 1. Notice the different  $w$  ranges on left and right panels. Different data sets reported in a given article are represented in all panels by identical symbols of different colors.

The coexistence curve and the cloud point curve are identical only for binary solutions comprising a solvent and a mono-disperse polymer. In this case there is no fractionation upon demixing. In contrast, for a polydisperse solution the chain length distribution of the minority phase produced upon demixing is modified with respect to the mother phase because longer chains tend to precipitate first. The composition of the minority, nascent phase is specified by the so

called shadow curve<sup>[10–12]</sup> that is difficult to characterize experimentally. Thus, in distinction to the binodal, the cloud point curve does not specify the composition of coexisting phases via the lever rule. Furthermore, the minimum of the cloud point curve, known as the precipitation threshold, is not identical to the LCST. For further details see Refs. [10–12]. The practical importance of these distinctions depends on the mixing free energy and the distribution of chain lengths. It is



nevertheless necessary to bear them in mind noting that the observed  $T_{\text{dem}}(w)$  may differ from the equilibrium curves described above because non-equilibrium effects play a role in the exploration of phase boundaries. Recall that probing the onset of demixing via turbidity measurements, DSC and similar methods requires a finite amount of minority phase. For example, the turbidity is due to formation of nascent minority phase in the form of polymer aggregates. Since the

**Figure 2.** a) A schematic depiction of a phase diagram exhibiting a LCST. The coexistence curve is drawn as a full line, the spinodal as dashed line and the LCST is indicated by a filled circle. A temperature quench from the homogenous, one-phase region into the metastable region between the binodal and the spinodal results in demixing via nucleation and growth [N&G]. It occurs in typical, off-critical, turbidity measurements. A temperature quench into the unstable region within the spinodal curve gives rise to spinodal decomposition [SD]. It was invoked in the studies by Inomata et al.,<sup>[101]</sup> Balu et al.,<sup>[49]</sup> and by Meier-Koll et al.<sup>[50]</sup> b) The binodals and c) spinodals predicted by the phenomenological free energies proposed by Afroze et al.<sup>[29]</sup> and Rebelo et al.<sup>[27]</sup> as well as by the model of Okada and Tanaka.<sup>[66]</sup> In each case the curves are specified for  $N=100$  and  $N=1000$ . Note that the free energy of Afroze et al. predicts a UCST at around  $T_{\text{UCST}} \approx 15^\circ\text{C}$ . The free energy of Rebelo et al. and the model of Okada and Tanaka predict an UCST at  $T_{\text{UCST}} > 100^\circ\text{C}$ . (not shown). The calculation of the curves of the Okada and Tanaka model utilized the parameters used by these authors<sup>[66]</sup> namely  $\Theta_0=555$  and  $\lambda_0=0.002$  for  $N=100$  and  $\Theta_0=565$  and  $\lambda_0=0.003$  for  $N=1000$ . The free energies are formulated in terms of monomer volume fraction  $\phi$ . The demixing curves are thus first obtained in terms of  $\phi$  and then converted to  $w$  utilizing  $w=1.1\phi/[(1-\phi)+1.1\phi]$  assuming mass densities of  $1.1\text{ g cm}^{-3}$  (PNIPAM) and  $1\text{ g cm}^{-3}$  (water).

solution is homogenous at the binodal, turbidity typically occurs when the system is off-critically quenched into the metastable region between the binodal and the spinodal, where demixing occurs via nucleation and growth<sup>[13,14]</sup> (cf. label [N&G] in Figure 2a). For aqueous PNIPAM solutions the quench typically involves an abrupt increase in the temperature,  $T$ . The rate of nucleation and the amount of minority phase increase with the extent of penetration into the metastable region<sup>[15]</sup> as controlled by the depth of the  $T$  quench with respect to the binodal,  $\Delta T$ . Larger  $\Delta T$  thus facilitate measurements. On the other hand, smaller  $\Delta T$  are desirable in order to accurately characterize the cloud point curve and the binodal. As we shall shortly elaborate this is an important issue.

### 3. Experimental Factors Contributing to Diversity

The differences between the reported phase diagrams arise in part from “technical” experimental issues. These fall into two main categories concerning: the measurement techniques (see Section 3.1) and the characteristics of the polymer as well as the preparation of the sample (see Sections 3.2 and 3.3). The details, while making for somewhat tedious reading, are useful for identification of trends as well as the design of future experiments.

#### 3.1. Measurement Issues

In this subsection we discuss three issues: the effect of the  $T$  scan rate and range, the choice of wavelength in optical measurements, and the criterion utilized to identify  $T_{\text{dem}}$ . The determination of the demixing curve typically involves heating/cooling the sample at a finite rate that varies in

practice between  $0.025 \text{ K min}^{-1}$  to  $1 \text{ K min}^{-1}$ . The rate affects the obtained demixing curves as evidenced by two observations. One concerns the difference between transmittance vs  $T$  plots as the heating rate is varied. Boutris et al.<sup>[16]</sup> compared the transmittance profiles for heating rates varying between  $5 \text{ K min}^{-1}$  to  $0.02 \text{ K min}^{-1}$ . The profiles obtained at  $5 \text{ K min}^{-1}$  were up-shifted by  $\approx 11 \text{ K}$  with respect to the profiles obtained at  $0.02 \text{ K min}^{-1}$ . Increasing heating rate from  $0.02 \text{ K min}^{-1}$  to  $0.2 \text{ K min}^{-1}$  resulted in a reduced up-shift of ca.  $1 \text{ K}$ . Similar observations were made by Kawaguchi et al.<sup>[17]</sup> who noted that the transmittance curve was independent of the scan rate below  $0.025 \text{ K min}^{-1}$ . A related point concerns deviations between the transmittance profiles obtained upon heating and upon cooling. For a scanning rate of  $1 \text{ K min}^{-1}$  Fujishige et al.<sup>[18]</sup> reported a higher transmittance for the heating curve while Zheng et al.<sup>[19]</sup> and Tong et al.<sup>[20]</sup> reported essential overlap for a scanning rate of  $0.033 \text{ K min}^{-1}$ . Ray et al.<sup>[21]</sup> also observed transmittance curve differences upon heating and cooling at  $1 \text{ K min}^{-1}$  with the additional ingredient that the effect varied with meso diad value of the polymer. While the issue received less attention for DSC experiments, van Durme et al.<sup>[22]</sup> reported that heating and cooling curves obtained at a scan rate of  $\pm 1 \text{ K min}^{-1}$  coincide when the maximal temperature of the scan was kept below  $32^\circ\text{C}$ . For higher maximal  $T$  the remixing exotherm was lower than the demixing endotherm and the difference increased as the heating rate decreased from  $2.5 \text{ K min}^{-1}$  to  $0.2 \text{ K min}^{-1}$ . Similarly, Xia et al.<sup>[23]</sup> reported that varying the scan rate between  $0.25 \text{ K min}^{-1}$  to  $1 \text{ K min}^{-1}$  did not affect the position of the endotherms' peak, but samples of low polydispersity developed an extra peak when maintained at higher  $T$  before the next heating scan. While reduced, this extra peak persisted even after prolonged incubation at  $10^\circ\text{C}$ . Likewise, the scattering intensity profiles upon heating and cooling as obtained using a microfluidic device of Zhou et al.<sup>[24]</sup> with a scan rate of  $\pm 0.5 \text{ K min}^{-1}$  were essentially identical. Finally, Otake et al.<sup>[25]</sup> found agreement between DSC and visually determined  $T_{\text{dem}}$  obtained at a heating rate of  $1 \text{ K min}^{-1}$  however the values obtained upon cooling were typically  $1 \text{ K}$  lower. Overall, while the results vary with the technique and the experimental protocol they suggest that fast scan rate and heating to  $T > T_{\text{dem}}$  tend to produce hysteresis. The effect of the scan rate may be related to the quench depth discussed in Section 2. We will return to the effect of the  $T$  range in Section 4.

The second issue we address concerns optical measurements. Different techniques were utilized to obtain demixing curves: transmittance,<sup>[16–18,20,22,23,26–28]</sup> scattering intensity at different angles,<sup>[24,26,28–30]</sup> and refractometry.<sup>[31]</sup> The transmittance and scattering intensity measurements rely on the light scattered by polymer aggregates having a refractive index differing from that of the surrounding solution. In turn, the scattering intensity varies with the wavelength  $\lambda$  and with the  $\lambda$ -dependent refractive index. It is thus worth noting the differences among the  $\lambda$  of the light sources utilized:  $500 \text{ nm}$ ,<sup>[16,18,23]</sup>  $632 \text{ nm}$ ,<sup>[19,20,26,27]</sup>  $615 \text{ nm}$ ,<sup>[22]</sup>  $650 \text{ nm}$ ,<sup>[17]</sup> and  $654 \text{ nm}$ .<sup>[28]</sup>

Finally, the values of the demixing temperature obtained from often used DSC and turbidity measurements depend on

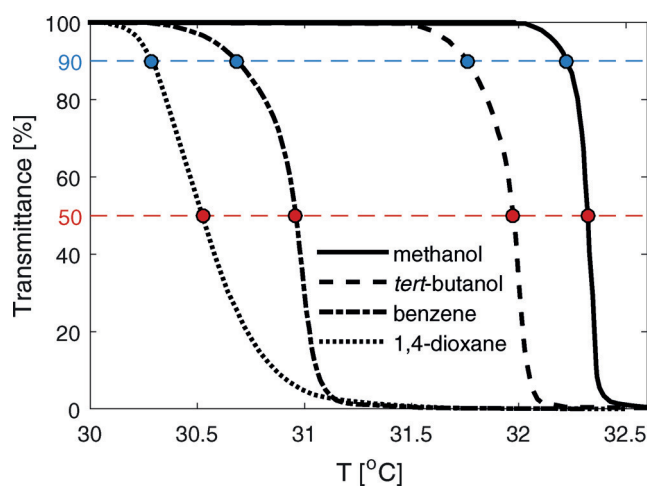


**Figure 3.** The relative transmittance curves obtained for PNIPAM samples of  $M_w \approx 50 \text{ kDa}$  and  $w \approx 0.05$  synthesized using AIBN in different solvents listed in brackets:  $M_w = 6.45 \times 10^4$  (methanol);  $M_w = 5.17 \times 10^4$  (*tert*-butanol);  $M_w = 4.65 \times 10^4$  (benzene);  $M_w = 5.18 \times 10^4$  (1,4-dioxane) redrawn after Figure 2 of Kawaguchi et al.<sup>[17]</sup> These authors identify  $T_{\text{dem}}$  with 10% reduction of the transmittance, i.e., 90% transmittance (blue circles). When the transmittance varies slowly with  $T$  the choice of criterion can have a significant effect as seen from the comparison to  $T_{\text{dem}}$  identified with 50% reduction (red circles).

the criterion utilized to determine  $T_{\text{dem}}(w)$ . This factor combines with instrumental sensitivity to affect the conclusions. Note that the choice of criterion affects  $T_{\text{dem}}$  obtained from a given data set (Figure 3) as well as the agreement between  $T_{\text{dem}}$  determined by different techniques. Boutris et al.<sup>[16]</sup> identified the transition with a 10% reduction of the transmittance and with the maximum of the derivative of the DSC heating endotherm. For a heating rate of  $0.2 \text{ K min}^{-1}$  they report agreement between  $T_{\text{dem}}(w)$  obtained by DSC and transmittance except for low  $w$  where the DSC  $T_{\text{dem}}(w)$  curve is lower. Afroze et al.<sup>[29]</sup> utilized the first deviation from the base line for both DSC and transmittance and found that the optical  $T_{\text{dem}}(w)$  curve is lower. Similar results were reported by Qiu et al.<sup>[32]</sup> and Xia et al.<sup>[23]</sup> who identified the transition with 50% transmittance and with the maximum of the DSC endotherm. Van Durme et al.<sup>[22]</sup> identified the transition point with 2% reduction in the transmittance and utilized two different criteria for extracting the  $T_{\text{dem}}$  from DSC based on two thresholds of the deviations from the extrapolated base line:  $0.01 \text{ J g}^{-1} \text{ K}^{-1}$  and  $0.1 \text{ J g}^{-1} \text{ K}^{-1}$ .  $T_{\text{dem}}$  obtained with the  $0.1 \text{ J g}^{-1} \text{ K}^{-1}$  criterion agreed with the optical results while the  $0.01 \text{ J g}^{-1} \text{ K}^{-1}$  threshold lead to a demixing curve lower by  $3 \text{ K}$ . Shi et al.<sup>[30]</sup> identified  $T_{\text{dem}}$  with the intersection of the two tangent lines, below and above the upturn in scattering intensity.  $T_{\text{dem}}$  obtained from laser light scattering was lower by roughly  $0.5 \text{ K}$  in comparison to the results acquired using their microfluidic device. Overall, the different criteria reflect an arbitrary compromise between early detection of nascent phase and experimental resolution, bearing in mind that the experimental curves vary with the sample.

### 3.2. The Sample Preparation

Two points are grouped in this subsection: The sample drying procedure and the dissolution protocol. Regarding the first point recall that the demixing curves are typically specified in terms of weight fraction  $w$  as obtained by dissolving a weighted sample of “dry” PNIPAM. The water content of the polymer sample utilized affects  $w$  and thus the demixing curve. This factor is especially significant for concentrated solutions. The drying procedure can thus have an important effect as demonstrated by Boutris et al.<sup>[16]</sup> who found that thermogravimetric analysis of solutions prepared from “dry” PNIPAM revealed up to 40% discrepancy between the nominal and actual  $w$ . In contrast van Durme et al.<sup>[22]</sup> dried polymer samples under vacuum for 48 h at 130 °C and then verified that the water content was below 0.2% using thermogravimetric analysis. The drying procedure is described only by some authors and varies widely. For example, Xia et al.<sup>[23]</sup> dried samples to constant weight under vacuum at 60 °C while Kawaguchi et al.<sup>[17]</sup> dried their samples at 80 °C under vacuum for 12 h.

Concerning the dissolution protocols note that preparing aggregate-free, homogenous aqueous PNIPAM solutions is also a possible issue, especially for high  $w$ . Again, the procedures are not always specified. Afroze et al.<sup>[29]</sup> equilibrated solutions at room temperature for several weeks. Van Durme et al.<sup>[22]</sup> stored their samples in a refrigerator for at least a week to ensure mixture homogeneity. Rebelo et al.<sup>[27]</sup> Gomez de Azevedo et al.<sup>[26]</sup> and Pamies et al.<sup>[28]</sup> kept their sample solutions stirring for several hours and up to several days.

### 3.3. The Polymer Sample

The phase diagrams are sensitive to the structural characteristics of the PNIPAM samples. The roles of the polymerization degree  $N$  and the PDI are widely recognized. In addition, the nature of the end-groups, degree of branching and tacticity also affect the results. The synthesis origins of these issues and their control will be discussed in Section 8. In this subsection we survey the manifestations of these factors in the phase behavior.

#### 3.3.1. Tacticity

In the case of PNIPAM tacticity refers to the orientation of the amide side group with respect to the backbone. One distinguishes between isotactic, syndiotactic and atactic chains. These respectively have side groups located exclusively on the same side of the backbone, have alternating positions or have random orientations. The tacticity is often quantified by the fraction of “meso diads” i.e., two adjacent monomers having side groups with identical orientation. While atactic PNIPAM is soluble in water, syndiotactic and isotactic PNIPAM samples are poorly soluble.

An early exploration of the effect of tacticity on PNIPAM demixing was reported by Habaue et al.<sup>[33]</sup> who investigated samples obtained via radical polymerization with 2,2'-azo-

bis(isobutyronitrile) (AIBN) initiator and Lewis acid catalysts. They noted that the cloud point of the isotactic rich polymer was lower than that of the syndiotactic rich one. Importantly they observed that the meso diad content,  $m$ , in the absence of Lewis acid, was constant at  $m = 45\%$  for a variety of polymerization temperatures and solvents: tetrahydrofuran, methanol, dimethylsulfoxide, water and chloroform. This last point is important because early studies of PNIPAM phase diagrams did not specify  $m$ .

A systematic study of the effect of  $m$  on demixing was carried out by Ray et al.<sup>[21]</sup> It concerned PNIPAM samples synthesized by reversible addition-fragmentation chain transfer (RAFT) polymerization in the presence of Lewis acid catalysts yielding polymers with  $M_w/M_n$  varying between 1.2–1.3,  $M_n = 37 \pm 3$  kDa and  $m = 45, 47, 49, 51, 53, 57, 62, 66$ , and 72%. Their  $T_{\text{dem}}$  at  $w = 0.01$  decreased with increasing  $m$ , being 31 °C for  $m = 45\%$  and 17 °C at  $m = 66\%$ . The isotactic rich  $m = 66\%$  sample was soluble in water upon ultrasonification while the  $m = 72\%$  sample was insoluble.

The effect of  $m$  on PNIPAM demixing curves was investigated by Katsumoto and Kubosaki<sup>[34]</sup> using samples having  $M_n = 32 \pm 2$  kDa, with  $M_w/M_n$  ranging from 1.12 to 1.30 and  $m = 46, 60, 64\%$  obtained via RAFT polymerization with a Lewis acid catalyst. The  $T_{\text{dem}}(w)$  curves of the  $m = 60\%$  and  $m = 64\%$  polymers in the range  $7 \times 10^{-4} \leq w \leq 0.08$  occurred at lower  $T$  (Figure 4). They also exhibited a plateau in the

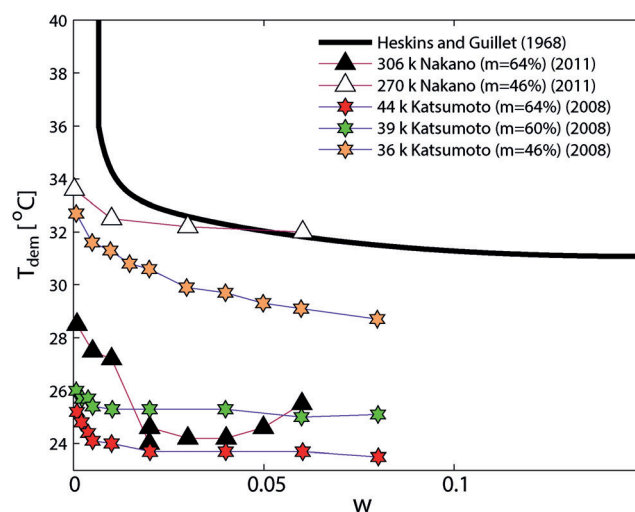


**Figure 4.** The effect of meso diads content,  $m$ , on the temperature  $T_{\text{dem}}$  vs. weight fraction  $w$  demixing curves.  $T_{\text{dem}}$  was estimated using the first derivative<sup>[34]</sup> or 50% reduction of transmittance curves.<sup>[36]</sup>

range  $0.02 \leq w \leq 0.08$  occurring at  $T = 24$  °C for  $m = 64\%$ . In addition, the transmittance curves of the  $m = 60\%$  and  $m = 64\%$ ,  $w = 0.01$  solutions were broader in comparison to their  $m = 46\%$  counterpart. This last observation motivated Nishi et al.<sup>[35]</sup> to study the phase separation of PNIPAM solutions with  $m = 46, 48, 51, 55, 56$ , and 58% using dynamic light scattering and small angle neutron scattering (SANS). Their results suggest that the coils shrink significantly prior to aggregation for the lower  $m$  samples while in the isotactic rich case chain shrinking and aggregation occur simultaneously.

Interestingly, Nakano et al.<sup>[36]</sup> reported that heating an isotactic rich  $m = 64\%$  PNIPAM solution results not only in an upturn of turbidity but also in a sol to gel transition as characterized by the descent velocity of a nickel ball. At  $w > 0.017$  the sol–gel transition occurred below  $T_{\text{dem}}$  defined by the onset of turbidity. Altogether the isotactic systems thus exhibited four states: transparent gel or sol as well as opaque gel or sol. In contrast, atactic PNIPAM undergoes no physical gelation.

Hirano et al.<sup>[37]</sup> investigated a syndiotactic-rich PNIPAM with  $m = 25\%$  obtained by radical polymerization in the presence of a Lewis base and fractionated by solvent-selective reprecipitation. It took two days to dissolve this sample in water. Plots of the temperature dependence of solution transmittance were recorded upon heating and cooling. They were remarkably different. Upon heating, the transmittance of the solution dropped sharply at  $32^\circ\text{C}$ . The upturn in transmittance upon cooling took place at a much lower temperature ( $15^\circ\text{C}$ ).

### 3.3.2. End-group Effects

A-(X)<sub>N-2</sub>-B linear chains comprise  $N-2$  identical repeat units and two terminal units, A and B, whose effect on the chains properties diminishes with increasing  $N$ . In the majority of experiments discussed in the following A is different from B. Furthermore, typically only one of the two terminal units is varied by using identical linkers/spacers and different end-groups.

The first observation of the end-group effect on the demixing was made by Otake et al.<sup>[25]</sup> They compared  $T_{\text{dem}}$  of two sets of PNIPAM samples: 1)  $M_w = 11\text{--}203$  kDa (PDI 2.0–3.4) prepared using AIBN initiator and thus having a neutral  $-\text{C}(\text{CH}_3)_2\text{C}\equiv\text{N}$  group linked to one chain end, and 2) PNIPAM  $M_w = 2100$  kDa (PDI 48.0) prepared using potassium persulfate initiator thus bearing charged sulfate  $\text{SO}_4^{2-}$  end-groups. The  $T_{\text{dem}}(w)$  of the  $-\text{C}(\text{CH}_3)_2\text{C}\equiv\text{N}$  terminated samples was essentially independent of MW and occurred 2 K below  $T_{\text{dem}}(w)$  of the  $\text{SO}_4^{2-}$  terminated polymer, a shift the authors attributed to initiator charge effects. The influence of  $\text{SO}_4^{2-}$  end-groups on aggregation in PNIPAM solution above the  $T_{\text{dem}}$  was later investigated by Chan et al.<sup>[38]</sup> as will be discussed in Section 4.

An early study of the effect of end-groups on  $T_{\text{dem}}$  was carried out by Chung et al.<sup>[39]</sup> This work focused on alkylterminated PNIPAM- $\text{C}_n\text{H}_{2n-1}$  with  $n = 3, 6, 8, 12, 18$  and with  $M_w = 8.9$  kDa. The polymers were prepared by radical polymerization in the presence of 2-aminoethanethiol as chain transfer agent. The terminal amine group of the polymer was reacted with alkyl chlorides yielding polymers with alkyl chains joined to PNIPAM by a  $-\text{SCH}_2\text{CH}_2\text{NHC}(=\text{O})-$  linker. For  $n = 3\text{--}8$  the  $T_{\text{dem}}$  decreased with increasing  $n$ . For  $n = 12$  and 18 there was evidence of micelle formation, an effect that may also influence  $T_{\text{dem}}$  of lower  $n$  samples. In a later work using the same linker Chung et al.<sup>[40]</sup> investigated also the effect of amino  $-\text{NH}_2$  and hydroxy  $-\text{OH}$  terminal groups on the  $T_{\text{dem}}$  of  $w = 5 \times 10^{-4}$  PNIPAM solutions. Both caused an increase in the  $T_{\text{dem}}$ , an effect that increased as the MW of the polymer decreased.

Interestingly the effect of the hydroxy terminus was stronger i.e.  $T_{\text{dem}}$  of the  $-\text{OH}$  terminated chains was higher than that of the  $-\text{NH}_2$  terminated ones.

Another study of the  $N$  dependence of end-group effects was reported by Furyk et al.<sup>[41]</sup> It compared  $T_{\text{dem}}$  of PNIPAM terminated by hydrophobic triphenylmethylamido  $-\text{CONHCPh}_3$  and by hydrophilic amido  $-\text{CONH}_2$  groups both joined via a  $-\text{C}(\text{CN})(\text{CH}_3)\text{CH}_2\text{CH}_2-$  linker. There was no MW dependence for  $M_w > 50$  kDa while for  $M_w < 50$  kDa the  $T_{\text{dem}}$  of hydrophobically modified PNIPAM was lower and grew with increasing MW.

A wider range of end-groups was explored by Xia et al.<sup>[23]</sup> using PNIPAM chains obtained by atom-transfer radical-polymerization (ATRP). The chains studied had one Cl terminated end and the second terminus carried five different end-groups,  $-\text{NH}_2$ ,  $-\text{NH}i\text{Pr}$ ,  $-\text{OEt}$ ,  $-\text{NHPH}$ ,  $-\text{OMe}$ , joined via  $-\text{CH}(\text{CH}_3)\text{C}(=\text{O})-$  linker. The  $M_n$  of the polymers ranged from 3 kDa to 18 kDa with PDI 1.13 or less.  $T_{\text{dem}}$  at low MW varied as  $\text{NH}_2 > \text{NH}i\text{Pr} \approx \text{OMe} > \text{OEt} > \text{NHPH}$ , with maximal difference of 8 K for  $M_w = 3$  kDa. All  $T_{\text{dem}}$  decreased with increasing MW and the difference between them diminished rapidly for  $M_w > 10$  kDa.

A study of chains with two identical terminal units was reported by Qiu et al.<sup>[32]</sup> who synthesized PNIPAM of  $M_w = 7$  kDa, 13 kDa, 26 kDa, and 45 kDa terminated with  $-\text{SC}(=\text{S})\text{SCH}_2\text{CH}(\text{CH}_3)_2$  or  $-\text{SCH}_2\text{CH}_2\text{C}(=\text{O})\text{OR}$  where R stands for  $\text{CH}_2\text{CH}_2\text{OH}$ ,  $\text{CH}_2\text{CH}_2\text{Cl}$ ,  $\text{CH}_2(\text{CH}_2)_4\text{CH}_3$ ,  $\text{CH}_2\text{CH}_2\text{CH}_2\text{CH}_3$ , or  $\text{CH}_2\text{C}\equiv\text{CH}$ . The polymers were prepared by end-modification of PNIPAM samples obtained via RAFT polymerization of *N*-isopropylacrylamide (NIPAM) with a symmetrical chain transfer agent that contained a  $-\text{C}(\text{CH}_3)_2\text{C}(=\text{O})\text{OCH}_2\text{CH}_2\text{OCH}_2\text{CH}_2\text{OC}(=\text{O})\text{C}(\text{CH}_3)_2-$  segment. This short chain was present in the middle of the polymer backbone for all samples studied. The MW dependence of  $T_{\text{dem}}$  at  $w = 5 \times 10^{-4}$ , as determined by turbidity and DSC measurements, exhibited the following trends:  $T_{\text{dem}}$  of  $-\text{CH}_2(\text{CH}_2)_4\text{CH}_3$ ;  $-\text{SC}(=\text{S})\text{SCH}_2\text{CH}(\text{CH}_3)_2$  terminated chains increased with increasing MW,  $T_{\text{dem}}$  of  $\text{CH}_2\text{CH}_2\text{CH}_2\text{CH}_3$  chains was independent of MW while  $T_{\text{dem}}$  of chains ending with  $\text{CH}_2\text{CH}_2\text{OH}$ ,  $\text{CH}_2\text{CH}_2\text{Cl}$ , or  $\text{CH}_2\text{C}\equiv\text{CH}$  decreased with increasing MW. The differences decreased with increasing MW and were negligible for  $M_w = 45$  kDa.

Liu et al.<sup>[42]</sup> investigated the behavior of PNIPAM chains obtained by RAFT polymerization using a chain transfer agent with  $-\text{S}(\text{C}=\text{S})\text{SCH}_2\text{CH}_3$  and di(propargyloxy) benzoate functionalities, used as handles for further modification. In all cases, end group effects were observed for polymers of low MW. They decreased with increasing MW and largely disappeared for  $M_w > 50$  kDa. Given the complex structure of the end-groups, specific observations reported in this study cannot be compared to trends emanating from the studies discussed above.

Overall, hydrophilic end-groups favor higher  $T_{\text{dem}}$  while hydrophobic end-groups are associated with lower  $T_{\text{dem}}$ . The end-effects diminish with increasing  $N$  and  $T_{\text{dem}}$  is essentially independent of  $N$  for  $M_w \gtrsim 50$  kDa. In comparing the different results note that  $T_{\text{dem}}$  reflects contributions from both terminal units allowing for linkers as well as end-groups. Note further that the terms hydrophobic/hydrophilic are used

intuitively and there is currently no unique method of quantifying the relative hydrophobicity of the end-groups.

### 3.3.3. Branching

The differences among the reported  $T_{\text{dem}}(w)$  obtained for PNIPAM samples having comparable tacticity and identical end-groups led Kawaguchi et al.<sup>[17,43]</sup> to investigate the role of the solvent used in the polymerization reaction. To this end they synthesized PNIPAM of comparable MW  $\approx$  100 kDa,  $M_w/M_n \approx$  1.1–1.2 and  $m = 48$ –49% using AIBN initiator in four different solvents: methanol, *tert*-butanol, benzene and 1,4-dioxane. The transmittance profiles and the resulting  $T_{\text{dem}}(w)$  curves revealed a systematic effect (Figure 3).

Synthesis in methanol and *tert*-butanol led to higher  $T_{\text{dem}}$  values compared to the ones obtained from samples synthesized in benzene and 1,4-dioxane. The authors suggested that the trend is due to differences in the degree of branching of the polymers. As discussed in Section 8.1.1, branches form during polymerization by chain transfer reactions, which occur more readily in solvents such as methanol. Chain transfer is facilitated when the growing polymer chain adopts a more compact configuration, that is, under poor solvent conditions.

### 3.4. A Comment on Data Collapse

The preceding sections suggest the possibility of systematic shifts in the demixing data. For example, a fast  $T$  scan rate may result in superheating thus leading to  $T_{\text{dem}}(w)$  that is higher than the equilibrium coexistence curve by a rate dependent  $T$  shift. Visually, Figure 1 indeed suggests the existence of families of curves having similar shapes. This impression is reinforced by Figure 5 where we identify five families of  $T_{\text{dem}}(w)$  curves that collapse upon vertically shifting the individual curves by a set-specific  $\delta T$ . We emphasize that the  $T$  values of the collapsed  $T_{\text{dem}}(w)$  curves are of limited significance because the “member” data sets were shifted so as to enhance overlap with a representative, unshifted reference curve.<sup>[\*]</sup> With this in mind, the collapsed curves identify differences in  $w$  dependence. It is useful to note the following observations: i) the data do not collapse onto a single curve; ii) Broadly speaking it is possible to distinguish between “flat”  $T_{\text{dem}}(w)$  with weak  $w$  dependence and “curved”  $T_{\text{dem}}(w)$  curves with a pronounced  $w$  dependence. This second category includes a family of curves displaying a clear minimum at  $w \approx 0.5$ ; iii) The membership of each collapsed family is not trivially correlated with MW or

another parameter specified in Table 1. The exception to this last statement is family (f) comprising of data of very low MW. We should add that we have no explanation for the depicted trends and that Figure 5 highlights the lack of consensus regarding the shape of the PNIPAM  $T_{\text{dem}}(w)$  curves. We shall return to this issue in the Discussion (Section 9).

## 4. Arrested Demixing and Hysteresis

Converting the experimental results to phase boundaries is hampered by observations of hysteresis and of arrested demixing. The second term refers to situations where initial chain aggregation results in long-lived particles, often named mesoglobules, such that the completion of the demixing is blocked and there is no macroscopic phase separation during the measurement period. These observations raise questions concerning the equilibration process and the nature of the equilibrium states. The relevant observations are presented below in chronological order under three subheadings grouping experiments concerned with: phase diagrams (Section 4.1), use of scattering techniques to probe aggregation behavior and chain configurations (Section 4.2), and utilization of fluorescence techniques to characterize microviscosity and dynamics within aggregates (Section 4.3).

### 4.1. Indications from Studies of Phase Diagrams

In an early paper Tong et al.<sup>[20]</sup> noted that heating PNIPAM  $M_w = 50$  kDa, 100 kDa,  $w = 0.31$  solutions to 31.7°C yielded long lived milky solutions. These did not segregate into two homogenous phases when maintained at this temperature for more than a week. Macroscopic phase separation involving coexistence of a transparent liquid and white gel was obtained upon centrifugation at 33°C.

Van Durme et al.<sup>[22]</sup> observed hysteresis effects using modulated temperature DSC. When PNIPAM  $M_w = 74$  kDa solutions of  $w = 0.5$  were heated to above 35°C the remixing upon cooling was slower than the demixing upon heating. They discussed this effect in terms of “partial vitrification”. The effect varied with the incubation time at the elevated temperature. For example, the remixing time of samples maintained at 70°C for 0, 1000, and 5000 min increased with the duration of the incubation reaching 1300 min for the 5000 min case. The long remixing time was attributed to slower diffusion of water into the dense PNIPAM regions.

A possibly related effect was noted by Xia et al.<sup>[23]</sup> who observed that maintaining PNIPAM solutions at  $T > T_{\text{dem}}$  led to the appearance of a new peak on the low  $T$  side in subsequent DSC scans. Incubation at 10°C for up to 600 min reduced this extra peak but did not eliminate it. Interestingly this effect was observed for low MW samples produced by ATRP but did not occur in samples produced by radical polymerization using AIBN initiator.

[\*] The families of  $T_{\text{dem}}(w)$  data were identified after inspection of the  $w$  ranges and the computed distribution of slopes at  $w = 0.05$  as obtained from data fitted using cubic spline interpolation. In the next step the set of  $T$  shifts,  $\{\delta T\}$ , of the data was calculated up to constant and separately for each family to minimize the mean square deviation between all pairs of family members using linearly interpolated  $T_{\text{dem}}(w)$  curves. A first estimate of the constant resulted from the requirement that the sum of deviations vanishes. The minimally shifted set was finally chosen to serve as reference curve with  $\delta T = 0$ .

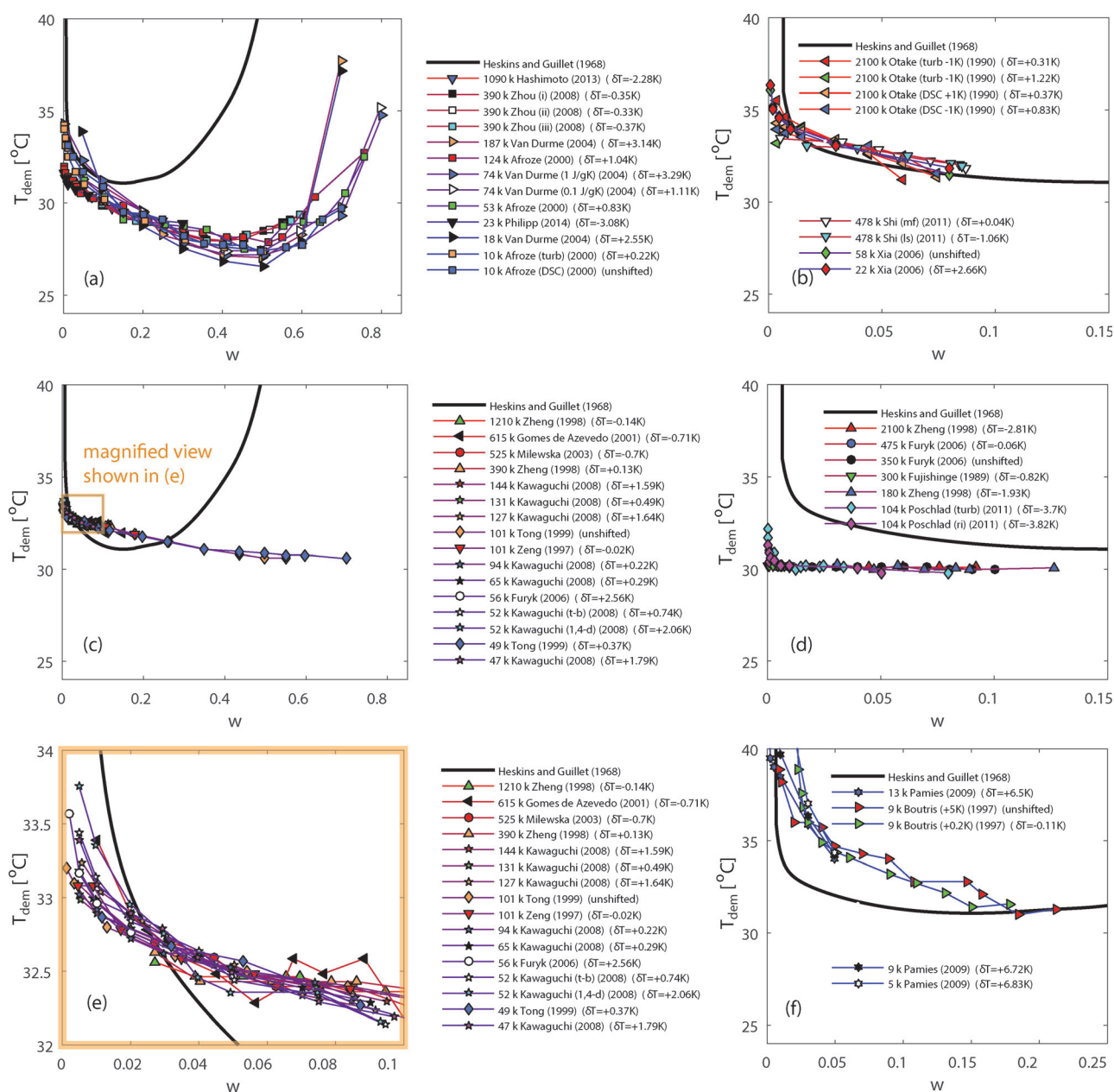


**Figure 5.** Families of demixing curves (a–d, f) can be nearly superimposed by up or down shifts along the  $T$  axis. The five families depicted are similar but not identical to the groups in the panels of Figure 1. The amplitude of the shift of each data set, denoted by  $\delta T$ , is specified in the legend of each panel. In each family the demixing curves are shifted towards one representative data set that retains its original  $T_{\text{dem}}$  and specifies the  $T$  range. The Heskins and Guillet demixing curve<sup>[7]</sup> is depicted for shape comparison. Note that the absolute  $T$  values are somewhat arbitrary and that the information is mainly contained in the shape of the curves and the  $w$  position of the LCST. The magnified view (e) of the low  $w$  range of panel (c) allows to better distinguish between the individual curves.

#### 4.2. Indications from Scattering Experiments

Direct evidence concerning arrested segregation upon heating of PNIPAM solutions was first reported by Gorelov et al.<sup>[44]</sup> who utilized light scattering and polymers synthesized using ammonium persulfate initiator thus having negatively charged  $\text{SO}_4^{2-}$  end-groups. The study concerned dilute solutions of  $w \approx 10^{-4}$ – $10^{-5}$  and MW in the 2000–9300 kDa range with  $\text{PDI} \lesssim 1.2$ . Their results indicated that the hydrodynamic radius  $R_h$  decreases by 30% with no aggregation upon increasing  $T$  from 25 °C to 33 °C. At higher  $T$  the chains

aggregated and beyond 33.5 °C the aggregation gave rise to mesoglobules, a term coined to describe dense, long-lived, mesoscopic spherical particles comprising several chains. The size of the mesoglobules initially increased with time and then leveled off to a stationary value that remained stable up to a few days at temperatures as high as 65 °C. The stationary size of the mesoglobules increased with decreasing heating rate and with increasing initial  $w$  of the solution. Dilution had no effect on mesoglobules solutions at 55 °C. The authors proposed an interpretation in terms of crossing the spinodal line at constant “moderately” high heating rate leading to

growing concentration fluctuations. Upon further heating “the collapse and aggregation of polymer chains kinetically arrests some correlation length of these fluctuations and this results in globules consisting of many chains with a size reflecting the effective correlation length.” The stability of the mesoglobules was attributed in part to low collision frequencies noting that some aggregation did occur at higher concentrations.

The interpretation proposed by Gorelov et al.<sup>[44]</sup> did not address the possible role of the charged end-groups and their effect on PNIPAM demixing. This issue was later explored by Chan et al.<sup>[38]</sup> using PNIPAM synthesized using the same initiator but having somewhat lower  $M_w \approx 550$  kDa. The size of the mesoglobules was studied using light scattering for solutions of higher  $w$ , in the  $w = 0.00025$ – $0.0045$  range, heated through the demixing curve to  $40^\circ\text{C}$ . The diameter of the mesoglobules varied linearly with  $w^{1/3}$ . The effect of ionic strength was weak for NaCl at concentrations up to  $0.003\text{ M}$  but the globule diameter grew steeply for higher ionic strengths, with  $\text{Ca}^{2+}$  leading to larger particles than  $\text{Na}^+$ . Increasing the NaCl concentration beyond ca.  $0.02\text{ M}$  resulted in macroscopic phase separation. Electrophoretic mobility demonstrated that the mesoglobules were negatively charged as expected in view of the sulfate end-groups. It was hypothesized that individual chains collapsed and then aggregated until colloidal stability was attained because of electrostatic interactions between the charged end-groups segregated to the mesoglobule surface.

Long lived collapsed globules of PNIPAM single chains were reported by Wu and Wang<sup>[45]</sup> who studied PNIPAM  $M_w \approx 10^4$  kDa with PDI = 1.02 and no charged end-groups using light scattering from extremely dilute solutions of  $w = 6.7 \times 10^{-7}$ . In the  $20^\circ\text{C}$ – $30.6^\circ\text{C}$  range both the radius of gyration,  $R_g$ , and the hydrodynamic radius,  $R_h$ , decreased with increasing  $T$  while  $R_g > R_h$  and the ratio  $R_g/R_h \approx 1.5$  was roughly constant. For  $30.6^\circ\text{C}$ – $32.4^\circ\text{C}$  the chain continued to contract but additionally  $R_g/R_h$  decreased from 1.5 to 0.56. Finally for  $T > 32.4^\circ\text{C}$  there was no change in  $R_g$  though  $R_h$  decreased slightly and both remained constant at the collapsed value for  $T > 35^\circ\text{C}$  when the globular density was  $0.34\text{ g cm}^{-3}$  corresponding to water content of 66%. There was no evidence of aggregation after incubation at  $35.9^\circ\text{C}$  for 2,000 min and both  $R_g$  and  $R_h$  remained constant after incubation at given  $T$  for 600 min. The chain dimensions on the cooling cycles were consistently smaller in comparison to the values observed upon heating. The authors concluded that such dilute solutions of collapsed globules are thermodynamically stable.

The demixing and aggregation of neutral PNIPAM  $M_w = 27.3$  kDa and  $160$  kDa solutions of  $0.00025 \leq w \leq 0.001$  in the  $20^\circ\text{C} \leq T \leq 50^\circ\text{C}$  range were studied using light scattering by Aseyev et al.<sup>[46]</sup> within a comparative investigation concerning also poly(*N*-vinyl caprolactam) (PVCL) and poly(vinyl methyl ether) (PVME). At relatively high  $w > 0.001$  reversible macroscopic phase separation occurred upon heating to above  $31^\circ\text{C}$ . Qualitatively different behavior was observed for more dilute solutions with  $w < 0.00025$ . In such solutions heating to temperatures above  $31^\circ\text{C}$  gave rise to dense spherical mesoglobules whose sizes grew with  $T$  and reached a plateau at  $36^\circ\text{C}$ – $41^\circ\text{C}$ . The size and the number of

mesoglobules at  $50^\circ\text{C}$  was not affected by subsequent dilution and remained constant over periods of up to 80 days. The size of mesoglobules obtained from solutions quenched to  $50^\circ\text{C}$  increased linearly with the initial PNIPAM concentration and was weakly affected by MW. Mesoglobules obtained by annealing were larger than ones obtained via quenching.

The hysteresis in PNIPAM phase demixing/remixing was investigated by Cheng et al.<sup>[47]</sup> using laser light scattering (LLS) and Fourier transform infrared (FTIR) spectroscopy. They investigated aqueous PNIPAM solutions of  $M_w = 1360$  kDa and  $M_w/M_n = 1.4$  at 14 temperatures between  $23.7^\circ\text{C}$  and  $40^\circ\text{C}$ . The solutions remained clear with no evidence of macroscopic phase separation over the full  $T$  range. The samples were allowed to reach thermal equilibrium at each measurement but the equilibration time was not specified. Static and dynamic LLS were used to measure  $R_g$ ,  $R_h$ , and the MW of  $w = 0.00023$  solutions. The FTIR results were obtained for  $w = 0.012$ . The LLS results concerning the heating behavior between  $25^\circ\text{C}$  and  $31.5^\circ\text{C}$  suggested chain contraction without aggregation as  $T$  increased. The MW was constant while  $R_g$  decreased. The ratio  $R_g/R_h$  was constant at ca. 1.35 between  $25^\circ\text{C}$  and  $30^\circ\text{C}$  but decreased to 0.5 upon heating to  $31.5^\circ\text{C}$ . Increasing  $T$  in the range  $32^\circ\text{C}$ – $36^\circ\text{C}$  gave rise to chain aggregation manifested by an increase in both MW and  $R_g$  while  $R_g/R_h$  increased to ca. 0.8. The aggregation reached a stationary state at  $T$  between  $37^\circ\text{C}$ – $40^\circ\text{C}$  where the MW,  $R_g$ , and  $R_g/R_h$  were constant. The cooling behavior was remarkably different. The MW,  $R_g$ , and  $R_g/R_h$  were constant upon cooling from  $40^\circ\text{C}$  to  $34^\circ\text{C}$ . Interestingly, cooling in the range  $34^\circ\text{C}$ – $32^\circ\text{C}$  led to an increase in both  $R_g$  and  $R_h$  with a decrease in  $R_g/R_h$  while MW was constant thus suggesting swelling of the aggregates. Further decrease in  $T$  results in an onset of decrease in MW evidencing aggregate dissolution. However the characterization of this range was complicated by the appearance of a slow mode suggesting objects with  $R_h = 1$ – $10\ \mu\text{m}$ . These did not disappear directly upon cooling to  $25^\circ\text{C}$  but disappeared when observed at  $25^\circ\text{C}$  after 1500 min incubation at  $4^\circ\text{C}$ . The LLS results were supplemented by FTIR measurements of absorbance at the  $1680\text{ cm}^{-1}$  to  $1560\text{ cm}^{-1}$  range. In  $\text{D}_2\text{O}$  the absorbance reflects two contributions of the C=O group: H-bonds to  $\text{D}_2\text{O}$ , giving rise to a band centered at  $1625\text{ cm}^{-1}$ , and H-bonds to H–N resulting in a shoulder at  $1650\text{ cm}^{-1}$ . The contribution due to  $\text{D}_2\text{O}$  bonds dominates at low  $T$  but decreases when  $T$  increases beyond  $32.5^\circ\text{C}$ .<sup>[48]</sup> The components of the IR bands due to the two species are constant in position and band shape and change only in intensity. The relative contribution was quantified by fitting the absorbance to two Gaussian peaks centered at  $1625\text{ cm}^{-1}$  and  $1650\text{ cm}^{-1}$ .<sup>[48]</sup> The fraction  $f$  of C=O groups forming H-bonds to H–N on other monomers was estimated from the ratio of the integrated area of the  $1650\text{ cm}^{-1}$  band and the total integrated area of the two C=O bands. They find  $f \approx 0$  up to  $32.5^\circ\text{C}$  and its subsequent increase with increasing  $T$ , approaching a plateau  $f \approx 0.11$  at  $40^\circ\text{C}$ . The cooling curve is above the heating curve in the range  $40^\circ\text{C}$ – $31^\circ\text{C}$ , i.e., the fraction of monomer–monomer H-bonds at a given  $T$  is higher upon cooling. The two curves merge for  $T < 30^\circ\text{C}$  where  $f \approx 0$ . The hysteresis effects were attributed to long-lived monomer–monomer H-bonds. One

should add that it will be interesting to study the evolution of the reported results as a function of the incubation time at a given  $T$ .

The demixing of PNIPAM  $M_w = 114$  kDa solutions of  $w = 0.01$ – $0.06$  quenched from room temperature to  $T = 34^\circ\text{C}$ ,  $36^\circ\text{C}$ ,  $40^\circ\text{C}$ , and  $45^\circ\text{C}$  was investigated by Balu et al.<sup>[49]</sup> using diffusive wave spectroscopy and small angle neutron scattering (SANS). Steady state was achieved in 10 min with evidence for the existence of dense roughly spherical particles whose radii decreased with increasing quench temperature: 330 nm for  $34^\circ\text{C}$  to 120 nm at  $45^\circ\text{C}$ . The corresponding PNIPAM volume fraction was estimated as  $\geq 0.9$ . Confocal microscopy images of adsorbed mesoglobules confirmed this picture. The stability of the mesoglobules was attributed to electrostatic repulsion between the mesoglobules which bear negative charge as revealed by electrophoretic mobility suggesting one surface charge per  $270\text{ nm}^2$ . This hypothesis is supported by the observation of macroscopic phase separation in the presence of LiCl at concentrations exceeding  $0.01\text{ M}$ . LiCl was utilized because at low concentrations it has little effect on  $T_{\text{LCST}}$  of PNIPAM. Importantly PNIPAM chains utilized in this study did not incorporate ionic groups since they were synthesized in 1,4-dioxane using an AIBN initiator. With this in mind, the charge on the mesoglobules was attributed to adsorption of residual ions at the globules surface. To rationalize the effect of the quench temperature on the mesoglobules size the authors argued that the mesoglobules arise from spinodal decomposition arrested by electrostatic repulsions preventing further growth of the PNIPAM domains.

The phase separation behavior of PNIPAM  $M_w = 25$  kDa solutions of  $w = 0.13$  at the  $15^\circ\text{C}$ – $50^\circ\text{C}$  range was studied by Meier-Koll et al.<sup>[50]</sup> using SANS. The scattering curves were modeled allowing for the sum of two contributions: concentration fluctuations described by the Ornstein-Zernike (OZ) scattering function<sup>[14]</sup> and scattering from interfaces following the Porod law. The first term described the  $15.6^\circ\text{C}$ – $32.9^\circ\text{C}$  range while the second term dominated at higher temperatures. The OZ correlation length diverges at  $33.1^\circ\text{C}$  indicating the spinodal at this  $w$ . Above  $33.1^\circ\text{C}$  the Porod law scattering intensity diminished with increased  $T$  and the mesoglobule surface to volume ratio  $S/V$  decreased. The obtained maximal  $S/V$  at the spinodal was  $S/V = 39\text{ mm}^{-1}$  thus suggesting domains of macroscopic scale in contrast to the results of Balu et al.<sup>[49]</sup> Time resolved SANS upon quenching the sample from  $20^\circ\text{C}$  to  $50^\circ\text{C}$  at a constant rate showed power law behavior  $S/V \sim t^\beta$  with time  $t$  but with  $\beta = 1.03$  up to  $t = 10$  min and  $\beta = 1.87$  for  $t = 83$  min.

The SANS measurements<sup>[49,50]</sup> were performed in deuterated water ( $\text{D}_2\text{O}$ ) to enhance contrast. It should be noted that the LCST of PNIPAM in  $\text{D}_2\text{O}$  is higher than in  $\text{H}_2\text{O}$  by ca.  $1\text{ K}$ .<sup>[51]</sup>

#### 4.3. Indications from Fluorescence Experiments

As noted above, the stability of PNIPAM mesoglobules increases with  $T$ , being highest at elevated temperatures  $50^\circ\text{C}$ – $80^\circ\text{C}$ , an effect described by van Durme et al.<sup>[22]</sup> as

“partial vitrification”. Kujawa et al.<sup>[52]</sup> investigated this phenomenon by monitoring fluorescence depolarization and non-radiative energy transfer (NRET) in solutions of fluorescently labeled PNIPAM  $M_w \approx 60$  kDa with  $w = 10^{-5}$ – $10^{-4}$ . The chains were labeled either by an energy donor naphthyl-*n*-octadecyl (PNIPAM-Np) or by an energy acceptor pyrenyl-*n*-octadecyl (PNIPAM-Py). These labels are hydrophobic and their association at low temperatures gave rise to small, swollen PNIPAM aggregates. However, the phenomenology of mesoglobule formation, as monitored by light scattering, was essentially unmodified: onset of chain aggregation upon heating was noted at ca.  $30^\circ\text{C}$  and the size of mesoglobules remained constant at  $T \geq 38^\circ\text{C}$ . As was observed by Balu et al.<sup>[49]</sup> the mesoglobules exhibited electrophoretic mobility indicative of a weak negative charge even though the PNIPAM chains utilized were neutral.

Two factors affect the fluorescence results: the local concentration of the fluorophores controls the probability of binary encounters and the microviscosity affects their mobility. The fluorescence depolarization reflects the tumbling motion of the labels and thus depends only on the microviscosity experienced by individual fluorophores. The NRET experiments probe the dynamics of encounters between different labels. The NRET trends at  $T < 30^\circ\text{C}$  are due to an increase in the local label concentration resulting from the mesoglobules formation. At higher  $T$  they mostly reflect the effect of microviscosity as it affects Brownian encounters. The NRET experiments took two forms. In one the PNIPAM-Py and PNIPAM-Np samples were mixed at low  $T$  thus leading to formation of mixed mesoglobules upon heating. In the second version the mesoglobules comprise initially pure PNIPAM-Py or PNIPAM-Np and the NRET probed the merging of mesoglobules or chain exchange between them. The results of all measurements were consistent with low, constant microviscosity at  $T < 30^\circ\text{C}$  with an upturn at  $32.5^\circ\text{C}$  reaching saturation value at  $36^\circ\text{C}$ . Interestingly, the “exchange–merging” experiments revealed a strong dependence on thermal history. The NRET at  $36^\circ\text{C}$  was weaker in samples that were first heated to  $80^\circ\text{C}$  as compared to samples that were first heated to  $50^\circ\text{C}$  or to samples that were gradually heated to  $36^\circ\text{C}$ . Overall these results suggest that mesoglobules below  $32.5^\circ\text{C}$  are in a fluid state while at higher temperatures the segment mobility within the mesoglobules is reduced thus leading to slower dynamics. This last effect is enhanced by incubation at temperatures above  $50^\circ\text{C}$ .

### 5. Macroscopic Phase Transition versus Arrested Demixing and Slow Coalescence

The experimental results discussed in Section 4 draw attention to two recurrent observations of i) long-lived, turbid solutions of PNIPAM mesoglobules, and ii) thermal hysteresis, i.e., behavior that depends on the thermal history of the sample. The two effects may reflect slow equilibration kinetics. Thus, one may hypothesize that the turbid solutions will eventually undergo macroscopic phase separation and that thermal history effects will disappear provided that the temperature scan rate is sufficiently low. Alternatively one

may postulate a richer phase diagram involving, for example, thermodynamically stable mesoglobules. In the following we outline a selection of pertinent theory results concerning these issues.

It is first helpful to recall that observations of arrested demixing and slow equilibration are not unique to PNIPAM. Similar effects were observed for other neutral water soluble polymers such as poly(*N*-vinylcaprolactam) (PVCL)<sup>[8]</sup> and poly(methyl vinyl ether) (PVME).<sup>[8,53]</sup> Mesoglobules were also observed in aqueous solutions of dendronized polymers having polymethacrylate backbones and ethoxy-terminated oligoethylene oxide side chains.<sup>[54]</sup> Such effects also occur in non-aqueous systems where hydrogen bonds are not involved. Equilibration times varying from days up to a month were reported for solutions of polystyrene in diphenyl ether.<sup>[55]</sup> Highly dilute solutions of polystyrene in cyclohexane undergo aggregation over a period of a week followed by slow precipitation lasting a comparable time.<sup>[56]</sup> Slowly coarsening polymer-rich droplets were observed in quenched solutions of polystyrene in diethyl malonate.<sup>[57]</sup>

The equilibration issue is intimately related to the demixing time scale. It assumes its simplest form for highly dilute polymer solutions. When such solutions are quenched into the biphasic region, individual chains first collapse into globules of radius  $R_{\text{collapse}}$  and then aggregate.<sup>[58]</sup> At first glance the aggregation of the globules is reminiscent of the coarsening of a mist of droplets resulting from similar quench of a binary mixture of simple fluids.<sup>[59]</sup> In this case droplets that come into contact merge very quickly to reduce their surface tension. The coarsening is described as diffusion limited aggregation where particles undergoing Brownian motion coalesce upon coming into first contact. The characteristic time for this process is the coagulation or Smoluchowski time [Equation (1)].<sup>[60]</sup>

$$\tau_{\text{coag}} = \frac{1}{8\pi DR_{\text{collapse}}c_0} = \frac{3}{4c_0} \frac{\eta}{k_B T} \quad (1)$$

Here  $c_0$  is the initial number concentration of collapsed globules of radius  $R_{\text{collapse}}$  whose translational diffusion coefficient, as given by the Stokes–Einstein equation, is  $D = k_B T / 6\pi\eta R_{\text{collapse}}$  where  $\eta$  is the solvent viscosity. Within this picture the aggregation is a diffusion controlled bimolecular reaction and  $\tau_{\text{coag}}$  is the time required for halving the number of particles. The applicability of this picture to polymers was first challenged in an experimental study<sup>[61]</sup> of polystyrene in cyclohexane solutions. In it, chain collapse was observed prior to aggregation but the onset of aggregation occurred after 500 s for a system with  $\tau_{\text{coag}} \approx 0.5$  s. The existence of such discrepancies was already noted by Smoluchowski who allowed for “slow coagulation” by phenomenologically introducing a fraction of collisions leading to fusion,  $\alpha \leq 1$ .<sup>[60]</sup> For slow coagulation  $\tau_{\text{coag}}$  is replaced by  $\tau_{\text{coag}}/\alpha$  and the  $\alpha < 1$  scenario was later attributed to potential barriers. Three directions emerged with regard to the origins of the slow coalescence of globules and mesoglobules: “topological” forces, “viscoelastic effects”, and electrostatic interactions.

The topological mechanism as formulated by Chuang et al.<sup>[62]</sup> is general and applies to collapsed globules of neutral

flexible chains irrespective of the solvent properties. It involves “topological” forces<sup>[63]</sup> arising because the two globules must intermingle while respecting topological constraints that chain trajectories do not cross. The coalescence is thus end-mediated and reminiscent of reptation. Full equilibration, including knot formation, is thus very slow. The interactions between the non-equilibrated chains are entropically unfavorable because of the statistical weight of configurations that are initially excluded because of topological constraints. The existence of such topological forces was demonstrated in computer simulations of two collapsed chains where the distance between the centers of mass was measured as a function of the attractive force applied to them.<sup>[62]</sup> While the monomer–monomer interactions were attractive the chains did not freely intermingle and the globule–globule interactions were repulsive on the time scale of the simulation. In this simulation the monomers interacted via Lennard–Jones potential thus leading to “classical” behavior with UCST, i.e., precipitation upon cooling. However, the physical argument rationalizing the results seems robust and applicable irrespective of the interaction potential. Indeed, the argument of Chuang et al.<sup>[62]</sup> was revisited by Jarkova et al.<sup>[64]</sup> within a detailed analysis of chain collapse in a two-state model having neutral water soluble polymers such as PNIPAM in mind. Within this model a monomer can freely interconvert between a hydrophobic *H* state and a hydrophilic *P* state. The chains considered were annealed, correlated, random *HP* copolymers, i.e., focusing on the case of a large energy cost of a boundary between *H* and *P* domains leading to long blocks. The *HP* conversion reaction was assumed to be unimolecular as in the Karlström model<sup>[65]</sup> and in distinction to the Okada–Tanaka<sup>[66]</sup> model where H-bond formation is a bimolecular reaction. In agreement with the early work of Grosberg<sup>[67]</sup> the authors find a first order collapse transition between a swollen coil and collapsed globule having a core–shell structure such that the core was *H* rich while the shell monomers were preferentially in a *P* state. The surface tension of the core–shell structure is reduced in comparison to a *H* homopolymer however this effect does not impart colloidal stability. The interactions between two globules are attractive in equilibrium when the trajectories of the two chains are equally distributed among the two globules. In qualitative agreement with the results of Chuang et al.,<sup>[62]</sup> kinetic stability may result from repulsive globule–globule interactions as they occur when the core relaxation is arrested, i.e., when a chain residing in one core is absent from the second core.

Our preceding discussion focused on collapsed single-chain globules and their slow coalescence as observed in highly dilute solutions following a deep *T* quench. Slow coarsening was also reported for deep quenches at higher polymer concentrations. Experimental observation of long lived mesoglobules, “mobile drop phase”, were rationalized by Tanaka invoking viscoelastic effects.<sup>[53,57,68]</sup> He argued that mesoglobule coalescence proceeds via reptation with characteristic time of  $\tau_{\text{rep}} \approx (\eta a^3 / k_B T) N \phi_{\text{pr}}^\alpha$  where  $a^3$  denotes the monomer volume,  $\phi_{\text{pr}}$  is the monomer volume fraction in the polymer rich droplet, and  $\alpha$  depends on the solvent quality being  $\alpha \approx 3/2$  for an athermal solvent and  $\alpha = 7/3$  for a  $\Theta$

solvent.<sup>[14]</sup> Note that  $\tau_{\text{rep}}$  increases with the quench depth  $\Delta T$  that affects the time dependent  $\phi_{\text{pr}}$ . Within this view coalescence is inefficient when  $\tau_{\text{rep}}$  is much longer than the collision time  $\tau_{\text{col}}$ ,  $\tau_{\text{rep}} \gg \tau_{\text{col}}$ , and two mesoglobules collide as elastic bodies. In turn  $\tau_{\text{col}}$  for two particles of radius  $R$  and mass  $m$  whose interaction range is  $r_0$  can be estimated via  $r_0/\langle v \rangle \lesssim \tau_{\text{col}} \lesssim r_0^2/D$ . The lower bound is set by the time to traverse  $r_0$  with the average velocity of Brownian particles  $\langle v \rangle \approx k_B T/m$  and the upper bound corresponds to the time to diffuse a distance  $r_0$  as set by the diffusion coefficient  $D = k_B T/6\pi\eta R$ . Following Tanaka one should however note that the viscoelastic mechanism does not explain the repression of aggregation due to van der Waals attraction.<sup>[53]</sup>

The viscoelastic effect as discussed above with regard to mesoglobules is expected to occur upon quenching of solutions below the overlap threshold,  $\phi < \phi^*$ .<sup>[69,70]</sup> Such effects were also invoked in discussing relatively long-lived transient structures occurring upon quenching of solutions at higher concentrations below the critical composition  $\phi_c$  i.e., initial states with  $\phi^* < \phi < \phi_c$ . In this case the quench initially resulted in network-like structure formed by the minority, polymer-rich phase and the solvent rich domains.<sup>[53,57]</sup> The structure and its evolution was discussed in terms of a transient gel arising because of entanglements and intra-chain attraction in poor solvents. On short time scales the overall volume of the gel is basically constant and chain–chain attraction in concert with connectivity constraints leads to microphase separation.<sup>[71]</sup> In contrast to mesoglobules, such network-like structures were not yet reported for PNIPAM solutions.

A different approach, applicable to water soluble polymers having neutral backbones, attributes the potential barriers to electrostatic interactions. As discussed already in Section 4 this hypothesis is supported by i) electrophoretic measurements indicating that the mesoglobules are negatively charged, and ii) the effect of the ionic strength on the mesoglobules size and colloidal stability. The charges may originate from ionic initiators giving rise to charged end-groups.<sup>[25,38]</sup> A second scenario, suggested by Balu et al.<sup>[49]</sup> attributes the charges to “adsorption of residual ions” at the surface of the mesoglobule. It was invoked when the initiator utilized was neutral and the PNIPAM chains were not expected to carry charges (see Section 4.2). Irrespective of the charges origin, the colloidal stability was discussed in terms of the Derjaguin–Landau–Verwey–Overbeek (DLVO) theory balancing van der Waals attraction with electrostatic repulsion.

Long-lived mesoglobules may reflect slow equilibration resulting in kinetic stability of thermodynamically unstable states. An alternative point of view postulates that globules and mesoglobules may be thermodynamically stable. This possibility emerges from theoretical analysis<sup>[72]</sup> of the *HP* side-chain model introduced by Vasilevskaya et al.<sup>[73,74]</sup> This is a coarse grained minimal model of a family of neutral water-soluble polymers, including PNIPAM, PVE and PVME, that comprise a hydrophobic main chain such that each repeat unit carries a side chain incorporating a hydrophilic group. In the case of PNIPAM, the hydrophilic group is an amide. Within this model each *H* unit in the flexible backbone is joined by

a phantom rod spacer to a *P* unit. Each *HP* unit is thus a “chemical dipole” characterized by the coordinates of the *H* unit and the orientation of the *HP* bond. In the interior of a collapsed globule the *HP* bonds are isotropically oriented. At the water interface the *HP* bonds are preferentially oriented because the *P* unit is hydrophilic. The surface free energy thus reflects three contributions: loss of orientational entropy, gain in energy due to preferential interactions of *P* units with water and a penalty term due to repulsive *PP* interactions. The surface free energy depends on the globular geometry that determines the solid angle explored by the *HP* dipole. As a result the surface free energy includes a surface tension contribution as well as bending elasticity terms that depend on the radii of curvature. The equilibrium states, as determined by minimization of the surface free energy, include spherical and cylindrical mesoglobules, vesicles and macroscopic phase separation. Their relative stability is determined by the surface tension and the bending moduli. The Maresov–Semenov<sup>[72]</sup> analysis suggests a possible rationalization of the observed long-lived mesoglobules as equilibrium structures. However direct confrontation with the observed phase diagrams of PNIPAM is challenging because values for the model parameters and their temperature dependence are currently unknown.

One should note that the ideas summarized above are not mutually exclusive. Disentangling the different contributions experimentally is, in general, difficult. The one noteworthy exception concerns electrostatic stabilization whose signatures are relatively straightforward to detect.

## 6. Type I versus Type II Phase Separations and the Mixing Free Energy: A Reminder

In discussing the phase diagrams of PNIPAM it is helpful to classify the phase separation behavior of polymer solutions according to the  $\phi$  value of the critical point,  $\phi_c$ , at the  $N \rightarrow \infty$  limit. For our purposes it is useful to distinguish between two cases: i) the familiar  $\lim_{N \rightarrow \infty} \phi_c = 0$  case<sup>[14]</sup> also referred to as type I behavior and, ii) the  $\lim_{N \rightarrow \infty} \phi_c = \text{const}' > 0$  case referred to as type II behavior<sup>[75,76]</sup> or “second type of phase separation”.<sup>[77]</sup> As we shall elaborate below there are indications that aqueous PNIPAM solutions exhibit type II behavior. In turn, this is of interest because type II behavior gives rise to distinctive PNIPAM brush structure thus permitting to confront bulk measurements with surface characterization.

Let us first recall the type I behavior, characteristic of the “standard” form of the Flory–Huggins theory.<sup>[14]</sup> Within it, the mixing energy per lattice site is  $\chi(T)\phi(1-\phi)k_B T$  where the Flory interaction parameter  $\chi(T)$  depends only on the temperature  $T$ . As long as  $\chi$  is independent of  $\phi$  the critical point of a polymer solution occurs at  $\phi_c \simeq 1/\sqrt{N}$  so that  $\phi_c \rightarrow 0$  for  $N \rightarrow \infty$  and phase separation takes place when  $\chi$  exceeds  $\chi_c \simeq \frac{1}{2} + \frac{1}{\sqrt{N}}$ . An empirical form often-used is  $\chi(T) = A + B/T$ . For this choice  $\chi(T)$  increases with increasing  $T$  when  $B < 0$ , thus giving rise to LCST, while for  $B > 0$  the trend is inverted, namely  $\chi(T)$  decreases with increasing  $T$  thus resulting in an upper critical solution temperature (UCST). Note here that

polymer theories are often formulated assuming a second virial coefficient of the form  $\nu \simeq (1 - \Theta/T)$  such that  $\nu$  changes sign at the  $\Theta$  temperature while all higher order virial coefficients are  $T$ -independent constants. This scenario corresponds to  $A = 0$  and  $B > 0$  and it does not allow for a LCST or type II behavior. The applicability of such theories to systems exhibiting LCST and/or type II behavior requires examination.

The realization of type II behavior requires replacing  $\chi(T)$  by an interaction parameter depending on both  $T$  and  $\phi$ , often denoted by  $g(\phi, T)$ .<sup>[10]</sup> The expressions for  $g(\phi, T)$  are often phenomenological utilizing variants of Equation (2) where  $B_i(T)$  are simple functions of a dimensionless absolute  $T$  [Eq. (3)] and  $b_{ij}$  are constants (see the Supporting Information).

$$g(\phi, T) = \sum_{i=0}^2 B_i(T) \phi^i \quad (2)$$

$$B_i(T) = b_{i0} + b_{i1}/T + b_{i2}T + b_{i3} \ln T \quad (3)$$

Alternatively one may invoke a physical model. A minimal physical model explicitly constructed to yield a type II behavior was proposed by de Gennes<sup>[77]</sup> having in mind polyethylene glycol. It was motivated by a now disputed observation of chain aggregation at high  $\phi$ . Within his “ $n$ -cluster” model the concentration dependence of  $g(\phi, T)$  is attributed to attractive interactions leading to stable clusters of  $n > 2$  monomers while binary monomer–monomer interactions remain repulsive. In molecular terms, a  $n$ -cluster may correspond to a micelle or a mixed helix. The formation of the  $n$ -clusters gives rise to an additional term,  $-\rho(T)\phi^n$  in the interaction free energy ( $\rho > 0$ ) thus leading to  $g(\phi, T) = \chi(T) + \rho(T)(1 - \phi^n)/(1 - \phi)$ . In the  $N \rightarrow \infty$  limit for an athermal solvent,  $\chi(T) = 0$ , the model predicts  $\phi_c = (n-2)/(n-1) \geq 1/2$  at  $\rho_c = n^{-1}[(n-1)/(n-2)]^n$  and demixing occurs for  $\rho > \rho_c$ , i.e., at  $\rho > \rho_c$  the solution segregates into two phases with monomer volume fractions  $\phi_-$  and  $\phi_+$  of identical exchange chemical potentials  $\mu(\phi_-) = \mu(\phi_+)$  such that  $\phi_- < \phi_c < \phi_+$ .

Additional candidates  $g(\phi, T)$  to describe type II behavior might be found among molecular models aiming to rationalize the phase behavior of neutral water-soluble polymers that owe their solubility in water to H-bonds.<sup>[78]</sup> Most of these models were formulated with PEG in mind and their parameters were determined by fitting its phase diagram. Within these “two state” models the monomers are assumed to interconvert between two states: a hydrophilic ( $P$ ) state that is favored at low temperatures and a hydrophobic ( $H$ ) state that is preferred at high temperatures. The chain is modeled as an annealed  $HP$  random copolymer. The two-state models differ in their identification of the interconverting states. In the Karlström model<sup>[65]</sup> the two states differ in their dipole moment and their interconversion involves an internal rotation. The models of Matsuyama and Tanaka,<sup>[79]</sup> Veytsman,<sup>[80]</sup> Bekiranov et al.,<sup>[81]</sup> and of Dormindotova<sup>[82]</sup> assume that the hydrophilic monomeric state forms one or more H-bonds to water molecules while the hydrophobic state does not. Thus far the only model aiming specifically at PNIPAM was formulated by Okada and Tanaka<sup>[66]</sup> who

modified the PEG model of Matsuyama and Tanaka to allow for cooperativity of the H-bond formation along the chains.

## 7. Evidence for Type II Phase Separation and PNIPAM Brushes

A qualitative indication that PNIPAM exhibits type II behavior is the  $N$  independence of its monomer volume fraction at the LCST,  $\phi_{\text{LCST}}$ . Among the four demixing curves (Figure 1a) spanning a wide  $0 < w \lesssim 0.8$  range<sup>[20,22,24,29]</sup> three<sup>[22,24,29]</sup> identify  $\phi_{\text{LCST}} \simeq 0.4\text{--}0.5$  for MWs spanning the 10 kDa  $\lesssim$  MW  $\lesssim$  390 kDa range. This suggests that  $\phi_{\text{LCST}}$  is essentially independent of  $N$  and that  $\phi_{\text{LCST}} > 0$  in the limit of  $N \rightarrow \infty$ . The demixing curve of Tong et al.,<sup>[20]</sup> the exception to the trend (Figure 1a), is monotonically decreasing with increasing  $w$  and thus provides no clear information on this issue.

The type II classification is also supported by phenomenological free energies of PNIPAM as implemented by Afroze et al.<sup>[29]</sup> and by Rebelo et al.<sup>[27]</sup> assuming special cases of Equations (2) and (3). Using the assumed form of  $g(\phi, T)$  allowed to fit their phase demixing data and, consequently, to determine the parameters of their models. At  $N \rightarrow \infty$ , Afroze et al. obtained  $\phi_{\text{LCST}}^\infty = 0.43$ ,  $T_{\text{LCST}}^\infty = 26.35^\circ\text{C}$  and concluded that PNIPAM follows type II behavior. Rebelo et al. did not address this issue but their phenomenological free energy leads to  $\phi_{\text{LCST}}^\infty = 0.13$  and  $T_{\text{LCST}}^\infty = 32.91^\circ\text{C}$  thus confirming the type II classification (Figure 2).

To our knowledge the  $n$ -cluster model was never utilized to fit PNIPAM phase diagrams. Its possible relevance to PNIPAM emerged indirectly from the work of Wagner et al.<sup>[83]</sup> on the self-consistent field (SCF) theory of planar brushes within the  $n$ -cluster model. Their analysis indicated that demixing at  $\rho > \rho_c$  can result in a vertical phase coexistence (Figure 6), i.e., the brush  $\phi(z)$  profile decreases with increasing altitude  $z$  but displays an inner dense region of  $\phi > \phi_+$  and an outer dilute region with  $\phi_- > \phi \geq 0$ . These regions are joined at a sharp boundary where  $\phi$  changes abruptly between  $\phi_-$  and  $\phi_+$ . Within the SCF theory the conclusion reflects the parabolic form of the exchange chemical potential of the brush monomers:  $\mu_{\text{brush}}(\phi_{\text{brush}}(z)) \sim (H_0^2 - z^2)$  where  $H_0$  is the brush height. Consequently, for polymers exhibiting  $n$ -cluster behavior the equilibrium condition  $\mu_{\text{brush}}(\phi_{\text{brush}}(z)) = \mu(\phi_+) = \mu(\phi_-)$  implies a discontinuous brush concentration profile such that  $\phi_+$  and  $\phi_-$  coexist only at a certain  $z$ . As  $\rho(T)$  increases the “phase boundary” moves towards the outer edge leading eventually to a brush comprising of a dense phase having a step-like distal boundary. The possibility of vertical phase separation within PNIPAM brushes was raised by Zhu and Napper<sup>[84]</sup> to rationalize their data on the collapse of PNIPAM brushes grafted to neutral, spherical latex particles immersed in water. Their results revealed a two-stage collapse upon increasing  $T$ . An “early collapse” took place below  $30^\circ\text{C}$  and did not result in flocculation. Upon raising the temperature above  $30^\circ\text{C}$  the additional brush contraction induced flocculation. This observation suggested that the colloidal stabilization imparted by the PNIPAM brushes survived the early collapse. It led Zhu

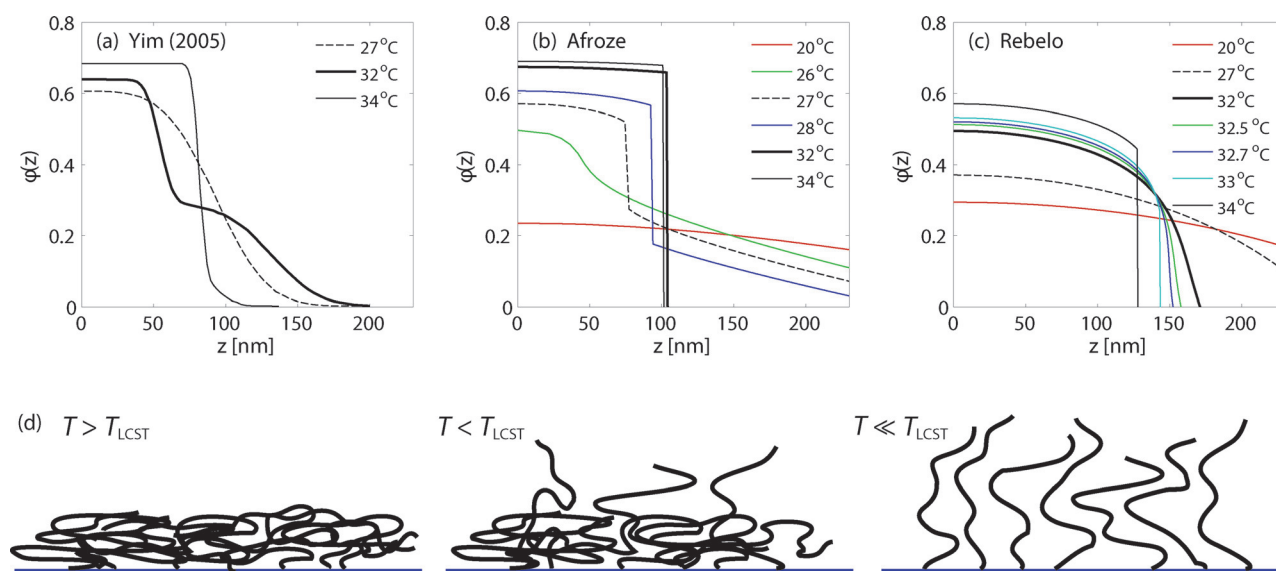


**Figure 6.** Volume fraction profile  $\phi(z)$  vs height  $z$  profiles of PNIPAM brushes as a) obtained from neutron reflectometry by Yim et al.,<sup>[89]</sup> b,c) obtained within the framework of the self-consistent field (SCF) theory employing the free energies of b) Afroze et al.<sup>[29]</sup> and c) Rebelo et al.<sup>[27]</sup> The SCF profiles were obtained numerically<sup>[88]</sup> on the basis of analytical results for flexible chain with monomer size  $a = 0.5$  nm assuming area per chain  $\Sigma = 4.76$  nm<sup>2</sup> and  $N = 2566$  corresponding to the reported experimental values of grafting density  $0.0021$  Å<sup>-2</sup> and  $M_w = 290$  kDa. The experimental  $\phi(z)$  profile at 27°C suggests a vertical phase coexistence and  $T_{LCST} > 27^\circ\text{C}$ . Its shape at 32°C suggests  $T_{LCST} < 32^\circ\text{C}$ . The experimental results are in qualitative agreement with the SCF profile based on the free energy of Afroze et al. which manifests a vertical phase coexistence at  $T = 27^\circ\text{C}$  consistent with the predicted  $\phi_{LCST}^\infty = 0.43$ ,  $T_{LCST}^\infty = 26.35^\circ\text{C}$ . In contrast the free energy of Rebelo et al. leads to  $\phi_{LCST}^\infty = 0.13$  and  $T_{LCST}^\infty = 32.91^\circ\text{C}$  with an onset of vertical phase coexistence at  $T = 32.9^\circ\text{C}$ . d) Drawing of the chain conformations corresponding to the volume fraction profiles in the various regimes.

and Napper<sup>[84]</sup> to interpret their results in terms of a vertical phase separation arguing that the exterior dilute brush imparts colloidal stability until it disappears upon increasing  $T$ . They further suggested that PNIPAM is described by the  $n$ -cluster model, an idea that is occasionally invoked to the present e.g. Plummer et al.<sup>[85]</sup> However, while the analysis of Wagner et al. was formulated for the  $n$ -cluster model, it is applicable to a wider set of models exhibiting type II behavior. These include, in particular, the free energy of Afroze et al.<sup>[29]</sup> Indeed, the SCF  $\phi(z)$  profiles of PNIPAM brushes as predicted on the basis of the Afroze free energy manifest a vertical phase separation<sup>[86–88]</sup> in semi-quantitative agreement with the neutron reflectivity results of Yim et al.<sup>[89]</sup> (Figure 6). It is interesting to note that the free energy of Rebelo et al.<sup>[27]</sup> does not reproduce these results. On the other hand, the Afroze free energy predicts a thus far experimentally unconfirmed UCST at  $\phi_{UCST} = 0.661$ ,  $T_{UCST} = 288.546$  K (15.396°C) (Figure 2).

## 8. Synthesis Overview

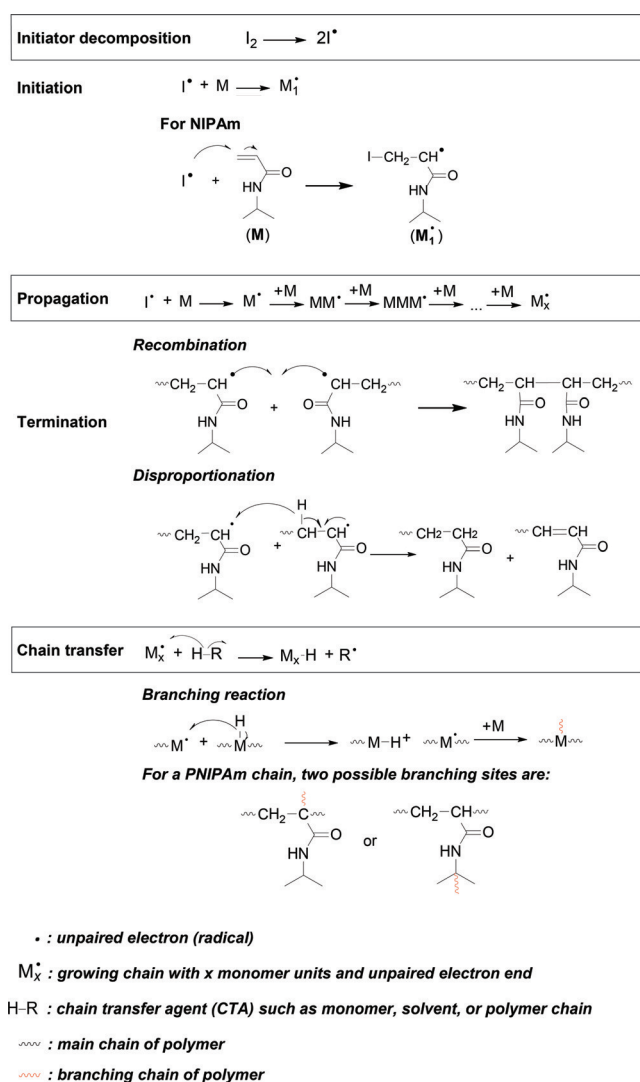
All PNIPAMs are not born equal! Polymer chemists know this intuitively, but theoreticians and physicists often overlook this point. In the following section, we recall a few key aspects of NIPAM polymerization and of the characterization of PNIPAM, with emphasis on features that may affect the elaboration of PNIPAM/water phase diagrams. The objective here is to give to readers unfamiliar with polymer chemistry the basic knowledge necessary to extract from the exper-

imental section of relevant articles a realistic description of the PNIPAM samples studied, beyond the specified nominal MW and polydispersity.

### 8.1. PNIPAM Preparation: Mechanistic Considerations

The vast majority of PNIPAM samples produced and studied are obtained by radical polymerization starting from a NIPAM solution containing a small amount of initiator. Ideally, the polymerization proceeds as depicted in Scheme 1. Heat, light, or a redox reaction triggers the decomposition of the initiator, “I<sub>2</sub>”, into a pair of free radicals I·, that is, a chemical species which bears an isolated electron and is obtained by homolytic cleavage of the electron pair forming the covalent bond in I<sub>2</sub> (top line in Scheme 1). The free radical I· then reacts with NIPAM to start a polymer chain. The chain grows by successive addition of the monomers until depletion of the monomer stock. The growing chain is de-activated eventually i) by coupling with another growing chain, which leads to a much longer chain (recombination) or ii) by disproportionation, that is, transfer of a hydrogen atom from one chain to another one, which gives two chains, one terminated with a double bond, the other with a saturated end group (Scheme 1, termination).

Alas, experimental evidence (wide molar mass distribution, lower molar mass than anticipated theoretically, etc) suggests that more chains are produced, compared to the chains expected based on the original initiator concentration. This implies that initiation of new chains takes place after all



**Scheme 1.** Free radical polymerization.

the initiator is consumed and throughout the course of the polymerization. New free radicals can form during the polymerization through removal by the chain radical ( $M_x^*$ ) of a hydrogen atom from another molecule ( $H-R$ ) present in the polymerization solution. When this happens, the growth of the chain is terminated, while the other molecule, now a radical  $R^*$ , can initiate the growth of a new chain. This process is known as “chain transfer” (Scheme 1).

One type of chain transfer to be considered results in the inadvertent formation of branched PNIPAM. It occurs when a chain radical reacts with a non-terminal unit of a polymer chain already formed. In PNIPAM the susceptible groups are  $CH_2$  and  $CH_3$ . The immediate result of this process is the termination of a growing chain and the reactivation of another chain, not at the chain end, but somewhere along the chain. NIPAM monomers react with this free radical resulting in the growth of a branch. This mechanism has been invoked by Kawaguchi et al.<sup>[17]</sup>

The prevalent type of chain transfer involves a small molecule, not the polymer chain itself. The entity intervening in chain transfer is usually called “chain transfer agent”

(CTA). Within the context of a review on the phase diagram of PNIPAM, CTAs, friends or foes, cannot be ignored.

### 8.1.1. CTA: The Enemy

Solvent molecules can act as CTAs, particularly if they possess weak C–H bonds that can be broken easily to release a hydrogen atom ( $H^*$ ) and produce a new free radical (homolytic cleavage of a covalent bond). Capture of this hydrogen atom by a chain radical stops its growth. Solvents able to undergo chain transfer, such as methanol, drive the polymerization towards PNIPAMs of low molar mass. To obtain polymers of very high molar mass, solvents such as *tert*-butanol, are preferred, since they do not form free radicals easily. Under these conditions, it is possible to obtain PNIPAM of high MW (> 106 kDa) and also, alas, a rather large PDI ( $\approx 2.0$  or higher).

The influence of the polymerization solvent on the molecular weight of the resulting PNIPAM is illustrated very well in Table 1 (columns 2 and 4). Benzene has been employed by some researchers. For safety reasons, this solvent is no longer available, at least in Europe and North America. It was replaced by toluene in a few studies. 1,4-dioxane is commonly used, in view of its polarity, suitable boiling point (101 °C, atmospheric pressure) for polymerization temperatures in the vicinity of 70 °C (decomposition temperature of AIBN), good solvent properties towards NIPAM and PNIPAM, and low toxicity compared to other ethers, such as tetrahydrofuran (THF). One caveat (see below), 1,4-dioxane is readily oxidized upon storage and needs to be purified and degassed before use.

### 8.1.2. CTA: The Friend

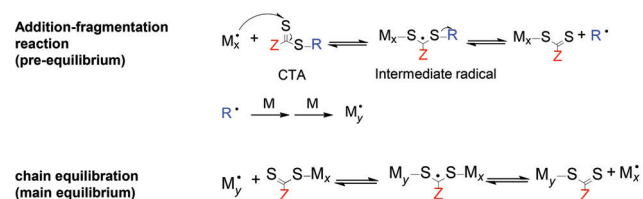
For polymer physicists and theoreticians familiar with THE polymer (polystyrene, of course), it may come as a surprise that until recently it was very difficult to prepare PNIPAM samples of low PDI. Polystyrene of narrow size distribution is readily obtained by living anionic polymerization. This method is highly effective in the case on nonpolar monomers (styrene). Polar monomers, such as NIPAM, are notoriously difficult to prepare by living anionic polymerization, due to side reactions, difficulties in finding appropriate polymerization solvents, etc. As described in the next section, PNIPAM of very low PDI (< 1.2) is routinely available nowadays, thanks to the advent of what are known as “controlled radical polymerizations” discovered in the mid-to late 1990s. Several controlled radical polymerization techniques exploit advantageously the unavoidable chain transfer reaction in radical polymerization, rather than trying to suppress it, using carefully designed “friendly CTA”s. There is a caveat, though, this method is effective only for the preparation of low molecular weight PNIPAM (MW < 80 kDa).

## 8.2. Controlled Radical Polymerization of NIPAM

The lack of control over polymer molecular weight stems directly from the inherent randomness of each step of the polymerization. In order to control the molecular weight, one must i) fix the total number of polymer chains, which can be done by choosing the relative concentrations of initiator and monomer, and ii) ensure that the monomers are distributed evenly among the growing chains, which demands that no living chain dies prematurely. This latter requirement, which can be satisfied in the case of anionic polymerization, seemed impossible to fulfill by radical polymerization. However, shrewd polymer scientists came to realize that the length of growing chains in radical polymerization can be controlled through the use of *reversible* reactions. This criterion defines the class of “controlled” radical polymerization.

### 8.2.1. Reversible Addition–Fragmentation Chain Transfer (RAFT)

The secret in RAFT polymerization is to add on purpose a CTA and to use it as a reservoir of radicals as described in Scheme 2 (see Ref. [90,91]). As in normal radical polymerizations, an initiator  $I_2$  is added to the polymerization mixture. Upon application of heat,  $I_2$  decomposes to form two free



CTA: *chain transfer agent used in RAFT polymerization, for example:*

$Z-S-S-R$  Dithioester CTA with *Z* activating group and *R* leaving group, or

$Z-O-S-S-R$  xanthate CTA with *Z* activating group and *R* leaving group.

**Scheme 2.** RAFT polymerization. Initiation and termination reactions are the same as those in the free radical polymerization (Scheme 1).

radicals  $I^\bullet$  that react with monomers and start the growth of polymer chains ( $M_x^\bullet$ ). At this point, the CTA interferes. It captures the growing chains  $M_x^\bullet$  and releases a new free radical  $R^\bullet$ . This transformation (pre-equilibrium in Scheme 2) results in the formation of a new CTA that carries a  $M_x$  chain instead of  $R$ . The captured  $M_x^\bullet$  chain is inactive or, rather, “dormant”. The radical  $R^\bullet$  is active of course and it promptly starts the growth of chains ( $M_y^\bullet$ ). When a living chain  $M_x^\bullet$  is captured by the CTA, the dormant chain  $M_x$  is reactivated, as depicted in the main equilibrium step (Scheme 2). The number of dormant chains equals the number of CTA molecules added. There exists termination, by recombination of chain radicals, but the number of dead chains is insignificant compared to the number of dormant chains. The dormant chains are inactive in the absence of free radicals, hence they are recovered at the end of the polymerization. This aspect of the RAFT polymerization implies that the end-groups of the recovered polymers originate from the CTA,

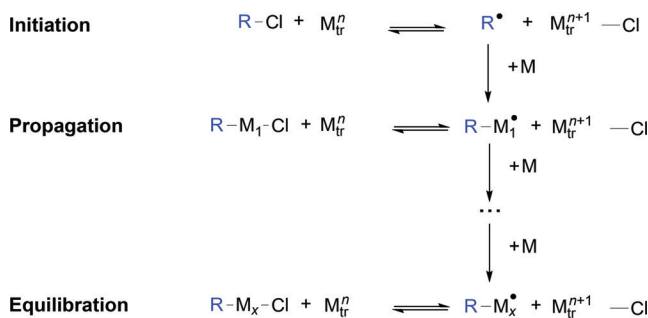
which is a useful feature to study the effect of end-groups on the phase diagram of PNIPAM.<sup>[32]</sup> Note the CTA can be hydrophobic or bear charged groups such as carboxylates. Such groups can have a significant effect on the phase diagram, particularly for PNIPAMs of low mass (< 10 kDa). For details on the RAFT polymerization, see Ref. [90,91].

RAFT polymerization of NIPAM is usually carried out with AIBN as initiator at a temperature 50°C to 70°C, in a solvent such as 1,4-dioxane. Dithioethers or trithiocarbonates are the most-frequently used CTAs (Scheme 2). Okamoto et al.<sup>[92]</sup> demonstrated that simultaneous control of the tacticity and molar mass of PNIPAM is achieved by addition of a suitable catalyst, such as yttrium triflate  $[Y(OTf)_3]$  to the RAFT polymerization mixture.

Currently, it is difficult to produce polymers of high molar mass by RAFT polymerization. In most cases, the MWs attainable span the 1 kDa to 50 kDa range. This may change, in view of the reported preparation of polyacrylamides of molar mass  $M_n \approx 106$  kDa of low PDI < 1.2 using a process named RAFT/MADIX (Macromolecular Design by Interchange of Xanthates)<sup>[93]</sup> where xanthates ( $R-O-C(=S)-S-R$ ) (Scheme 2) act as CTAs.<sup>[94]</sup> High MW copolymers of NIPAM were obtained under these conditions, but, curiously, the authors did not report the corresponding preparation of PNIPAM homopolymer.

### 8.2.2. Atom Transfer Radical Polymerization (ATRP)

The other controlled radical polymerization often used to prepare PNIPAM, known as atom transfer radical polymerization (ATRP), involves a *reversible chain termination* (in RAFT it is *reversible chain transfer* as the name indicates). In ATRP, a free radical  $R^\bullet$  is obtained from an initiator, such as  $R-Cl$  in Scheme 3, in the presence of a transition metal



$R-Cl$ : *organic chloride (initiator)*

$M_{tr}$ : *transition metal such as Cu, Fe, etc... (catalyst)*

$n$ : *oxidation degree of transition metal*

**Scheme 3.** ATR polymerization (ATRP).

species,  $M_{tr}^n$ . In the initiation process,  $R^\bullet$  and a halide radical ( $Cl^\bullet$ ) are formed. The transition metal species is converted to its oxidized form ( $M_{tr}^{n+1}-Cl$ ). The radical  $R^\bullet$  reacts with monomers to start chain propagation forming a polymer chain radical ( $R-M_x^\bullet$ ). By reaction with  $M_{tr}^{n+1}-Cl$ , the growing

chain  $R-M_x\cdot$  is converted to a “dormant” chain capped with a halide ( $R-M_x-Cl$ ) and the reduced form of the transition metal ( $M_{tr}^n$ ) is regenerated. The propagation/equilibration process (Scheme 3) continues, whereby the molecular weight of the polymer ( $R-M_x-Cl$ ) increases linearly with time. The polymerization stops when all the monomer is consumed. Under ideal conditions, all the chains have the same size and have a halide linked to one chain end. The other chain end ( $R$ ) originates from the initiator  $R-Cl$ . This feature of ATRP was exploited to study the effect of end-groups on the phase diagram of PNIPAM.<sup>[23]</sup> From the mechanism of ATRP it follows that in this study one chain end was variable ( $R$ ), the other chain end was  $Cl$  in all cases.

In summary, ATRP is a flexible polymerization method that yields polymers of low polydispersity. It is often used to prepare well-defined PNIPAM brushes grafted on solid substrates. Like RAFT polymerization ATRP is not suitable for the preparation of PNIPAM of high molecular weight ( $M_w > 50$  kDa). For PNIPAMs of low molecular weight, the choice between the two techniques is often driven by the expertise of a researcher in one method or the other. One of the drawbacks of RAFT polymerization is that it leads to slightly yellow to pink polymers, due to the dithioester end-groups that absorb light in the 300–400 nm spectral region. The dithioester end groups are sensitive to amines and other reagents, which can be a drawback in some cases, an advantage in others, for instance if further functionalization is required or to control end-group effects.<sup>[32]</sup> The end-groups introduced by ATRP (a chloride and an alkyl group) are usually stable and innocuous. The use of transition metals in ATRP can be seen as a drawback, especially if residual amounts of possibly toxic metal ions is of concern.

### 8.3. Practical Aspects of PNIPAM Preparation and Handling: How do They Affect the Phase Diagram of PNIPAM? Or How to Read the Experimental Section?

#### 8.3.1. Synthesis of PNIPAM

Many methods developed for the (standard) radical polymerization of NIPAM call for an organic solvent, which solubilizes NIPAM, PNIPAM, and the initiator. AIBN is used as initiator in most cases, but peroxide initiators may be employed, to introduce a specific end group or to allow changes of the polymerization temperature. This temperature must be set sufficiently high to decompose the initiator with generation of radicals (50–70 °C in the case of AIBN). NIPAM can also be polymerized in water using ammonium persulfate or potassium persulfate in the presence of activators to produce free radicals. In this case, heat is not required to generate free radicals. Polymerization can be conducted at room temperature or below. This method produces PNIPAM bearing negatively-charged end groups that cannot be ignored as they may affect the properties of PNIPAM solutions, as discussed in previous sections (see Sections 3.3.2, 4.2, and 5). It should be remembered that if the polymerization is carried out in water at a temperature higher than ca. 32 °C, the growing radical chain becomes insoluble in water. This can

induce undesired side reactions, such as crosslinking, as a consequence of the high local chain concentration<sup>[95]</sup> as discussed in detail in the context of PNIPAM microgel synthesis.<sup>[96]</sup>

Oxygen or peroxides present in the polymerization mixture also affect the polymerization outcome. Hence, it is well advised to remove oxygen from the polymerization solution (a process often called de-gassing or out-gassing) before initiation by heat. Peroxides often form in ethers, such as 1,4-dioxane or tetrahydrofuran, which are prone to oxidation. Polymerization solvents should be distilled and degassed immediately prior to polymerization. Of course, impurities in NIPAM must be removed by recrystallization (solvent: acetone/hexane mixture) when purchased from commercial suppliers. Precise information on purification of monomer and solvent should be given in addition to the polymerization conditions (temperature, time, concentrations, etc.). For reasons described above, the polymerization solvent is selected among good solvents for PNIPAM. The procedure implemented to recover the polymer from this solution should be described, as it affects the purity of the sample, its water content, etc.

#### 8.3.2. Fractionation of PNIPAM

In order to obtain polymers of high MW and narrow PDI, tedious fractionation of the polymerization product must be performed. This procedure involves selective precipitation of the polydisperse PNIPAM, as described by Wang et al.,<sup>[97]</sup> Zheng et al.<sup>[19]</sup> as well as Furyk et al.,<sup>[41]</sup> the original procedure is due to Fujishige et al.<sup>[98]</sup> In a precipitation, a concentrated solution of the polymer in a good solvent (very dry acetone) is added dropwise to a large volume of a poor solvent (very dry hexane), so that the polymer becomes insoluble as soon as a drop of the concentrated solution contacts the poor solvent. The insoluble polymer is recovered from the poor solvent by filtration and drying. The MW and PDI of the recovered sample are determined by gel permeation chromatography (GPC) or other suitable methods. This process must be repeated several times and often results in significant loss of polymer. It is followed by other manipulations, such as filtration through 0.5 micrometer filters.<sup>[97]</sup> Controlled precipitation of PNIPAM from acetone/hexane mixtures under conditions of controlled temperature was discussed by Zheng et al.<sup>[19]</sup> This process, although tedious, is the only known way to prepare PNIPAM of low PDI and high  $M_w > 100$  kDa.

The construction of accurate PNIPAM phase diagrams, as defined in the context of this Review, requires innovations in polymer synthesis and/or purification. PNIPAM of high molecular weight and narrow polydispersity should be made available on a large scale, either by de-novo polymerization or via large scale fractionation procedures. There is also an urgent need of a consensus on standards experimental conditions to determine the  $T_{dem}$  temperatures of thermosensitive polymers in solution, to facilitate the dialog among scientists using or studying this class of polymers.

## 9. Summary and Outlook

The leading features of the phase diagram of aqueous solutions of PNIPAM were identified by Heskins and Guillet<sup>[7]</sup> nearly 50 years ago: a LCST type behavior with precipitation upon heating to around 30°C. However, subsequent work (Table 1) failed to quantitatively reproduce their results or to reach a consensus. The reported  $T_{\text{dem}}(w)$  curves differ in absolute values and in shape (Figure 1). While it is possible to recognize “families” of  $T_{\text{dem}}(w)$  curves of similar form (Figure 5) this review did not identify a single “correct” phase diagram nor rationalize the origins of the  $T_{\text{dem}}(w)$  “families”.

Measurement issues are among the factors contributing to the differences among  $T_{\text{dem}}(w)$  curves. For example, criteria for onset of demixing vary and lead to demonstrable effect on the  $T_{\text{dem}}(w)$  curves as exemplified by the results of van Durme et al.<sup>[22]</sup> Differences in procedures, such as heating/cooling rates, also contribute. These factors are operational even for identical polymer samples. However the PNIPAM samples studied were obtained via synthesis protocols that often differed in the choice of initiator, solvent, purification procedure etc. The choice of protocol in turn gave rise to differences in sample characteristics such as polydispersity, end groups, branching and tacticity with corresponding effects on the phase boundaries. A more fundamental contributing factor concerns the detection of phase boundaries using techniques, such as turbidity measurements, that probe non-equilibrium effects. The interpretation of the turbidity data as an indicator of a two-phase coexistence curve is straightforward only when the onset of turbidity is followed by macroscopic phase separation on the time scale of the experiment. For PNIPAM solutions this condition is often unfulfilled thus posing a choice between two possible scenarios yet to be resolved: i) The turbid state is kinetically stable but thermodynamically unstable and will eventually phase separate given enough time. ii) The turbid state is thermodynamically stable reflecting a more complicated phase diagram including a “mesoglobular phase”.

In designing future experiments regarding PNIPAM phase diagrams it is useful to note the following observations: i) There are indications that mesoglobule stability reflects electrostatic contributions even for PNIPAM terminated by neutral end-groups. The contribution of this mechanism can be clarified by electrophoretic mobility measurements as well as via monitoring the effect of added salt on the mesoglobule stability. The use of LiCl to tune the ionic strength has been proposed<sup>[49]</sup> because it is known to induce minimal shift in the phase diagram of PNIPAM at concentration below 0.1M.<sup>[99]</sup> ii) Certain theoretical models predict equilibrium globules or mesoglobules having non-spherical geometry. There is thus an interest to image the particles in the turbid solution. Imaging is also of interest at higher  $w$  because of reports of transient network/sponge like structures. iii) When  $T$  scans are utilized it is useful to note that scan rates below 0.025 K min<sup>-1</sup> are apparently necessary to avoid hysteresis as manifested in differences between heating and cooling data or dependence of  $T_{\text{dem}}(w)$  curves on the scan rate. iv) The existing evidence for LCST at  $w \approx 0.5$  suggests the exploration of a correspond-

ingly wide  $w$  range. v) In studying demixing of high  $w$  samples it is necessary to allow for PNIPAM hygroscopicity and it is helpful to verify the composition of the PNIPAM powder by thermogravimetric analysis. vi) The reported observations suggest that heating to above 31°C–35°C is necessary in order to reach the “stable” mesoglobule regime. However, the precise boundaries of the “mesoglobular” domain remain to be mapped and the effect of  $w$  and  $N$  is yet to be systematically explored. vii) Some of the difficulties noted above are traceable to non-equilibrium aspects of the measurements utilized to map the phase boundaries. Such problems can be avoided by measuring equilibrium quantities. Of particular interest are the measurements of the ratios of volumes of the coexisting phases as a function of  $T$  for each  $w$ , an approach allowing to determine the coexistence curve.<sup>[10,55]</sup> While this method is time consuming and may require large amounts of polymer samples, its deployment minimizes the role of non-equilibrium effects. viii) Polymerization conditions, such as choice of solvent, were demonstrated to have an effect on the turbidity curves<sup>[17]</sup> and should be reported together with sample characteristics such as PDI and tacticity. ix) Inasmuch as the interest is in the “inherent” phase diagram of PNIPAM it is useful to study samples having MW > 50 kDa because in this range end-effects are negligible. Because of the evidence of type II behavior there is an interest in exploring high MW > 100 kDa. In the current state of the art this imposes the use of free radical polymerization and fractionation.

Turning now to “overall strategy”, recall that unambiguous determination of phase diagrams requires an interplay of theoretical modeling and experimental measurements.<sup>[10]</sup> The theoretical model, be it phenomenological or molecular, introduces an explicit free energy depending on adjustable parameters grouped into an interaction parameter  $g(\phi, T)$ . In turn, these adjustable parameters are determined by fitting to a particular set of experimental results. Once the adjustable parameters in  $g(\phi, T)$  are determined one may test the validity of the free energy by confronting calculated observable properties with additional experimental measurements and if necessary reiterate the process. In the case of PNIPAM the implementation of this process is at an early stage. The parameters of three free energies were determined by fitting to experimental  $T_{\text{dem}}(w)$  curves: The phenomenological models of Afroze et al.<sup>[29]</sup> and Rebelo et al.<sup>[27]</sup> were fitted to their respective experimental data and the molecular model of Okada and Tanaka<sup>[66]</sup> was fitted to the results of Rebelo et al.<sup>[27]</sup> The binodals and spinodals obtained from the three models differ significantly (Figure 5) but it is difficult to evaluate their relative merits in the absence of consensus with regard to the experimental  $T_{\text{dem}}(w)$ . Thus far there was no attempt to refine the adjustable parameters of the free energies using complementary experimental data, e.g., osmotic pressure measurements, scattering data of the single phase solution, spinodals curves etc.<sup>[10]</sup> It is however possible to demonstrate the initial stages of this approach utilizing reported results concerning the osmotic pressure<sup>[100]</sup> and the spinodal curves<sup>[49,50,101]</sup> of PNIPAM solutions. A comparison with the phenomenological models indicates that the predictions obtained from the free energy of Afroze et al. are in reasonable agreement with the spinodal points of Inomata

et al.<sup>[101]</sup> (Figure 7). The free energy of Afroze et al. also performs better in confronting the neutron reflectivity results regarding PNIPAM brushes<sup>[89]</sup> (Section 7 and Figure 6). On the negative side, it predicts a hitherto unobserved UCST at  $T_{UCST}$  (Figure 2) and the comparison to the osmotic pressure data of Nagahama et al.<sup>[100]</sup> (Figure 8) reveals a factor of ten

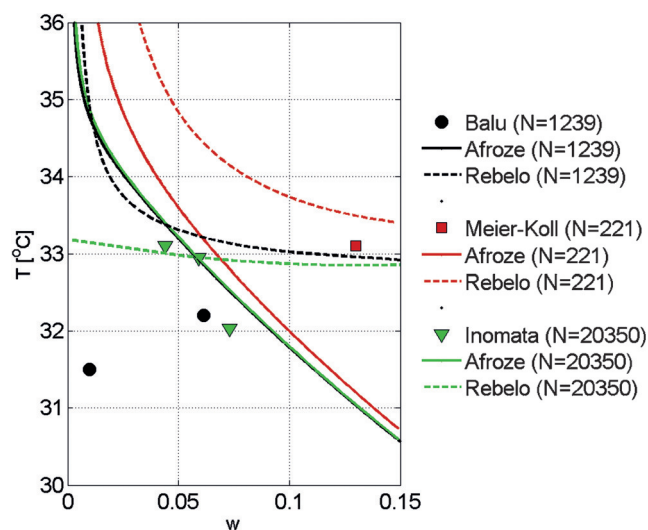


**Figure 7.** The spinodal points reported by Meier-Koll et al.<sup>[50]</sup> for  $M_w = 25$  kDa ( $N = 221$ ) by Balu et al.<sup>[49]</sup> for  $M_w = 138$  kDa ( $N = 1221$ ) and by Inomata et al.<sup>[101]</sup> for  $M_w = 2300$  kDa ( $N = 20350$ ) as compared to the spinodals calculated for these  $N$  values from the free energies of Afroze et al.<sup>[29]</sup> and of Rebelo et al.<sup>[27]</sup>

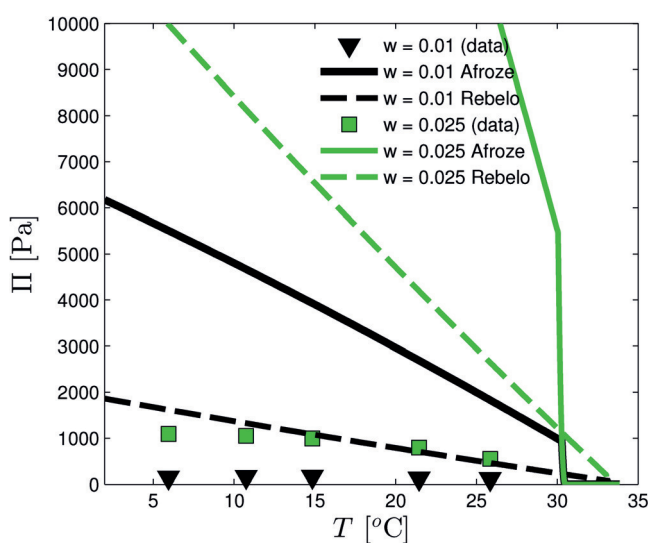


**Figure 8.** Osmotic pressure  $\Pi$  vs  $T$  for various  $w$  as measured by Nagahama et al.<sup>[100]</sup> for  $M_n = 360$  kDa ( $N = 3180$ ) compared to calculated values employing the free energies of Afroze et al.<sup>[29]</sup> and Rebelo et al.<sup>[27]</sup> using monomeric volume of  $v = 0.17$  nm<sup>3</sup>.

difference. Clear conclusion on the performance of the phenomenological free energies is thus currently impossible and the comparisons listed above only serve to illustrate the first step in the “overall strategy”. Insights regarding the molecular modeling of PNIPAM and the functional form of

$g(\phi, T)$  will eventually emerge from atomistic simulations of PNIPAM with explicit water. The simulation results may however depend on the choice of the water model and the force field describing PNIPAM<sup>[102]</sup> and the conclusions may vary with the definition of H-bond utilized.<sup>[103]</sup>

The elucidation of the phase diagram of aqueous solutions of free linear PNIPAM chains is a facet of the broader goal of the parametrization of the mixing free energy of PNIPAM. This, in turn, is an enabling step for addressing a wide variety of questions concerning an extended range of systems including gels and brushes of PNIPAM and its copolymers. This point is illustrated by a theoretical analysis of the harvesting of cell sheets cultured on PNIPAM brushes using the free energy of Afroze et al. to obtain numerical results.<sup>[104]</sup> The parametrization also provides an important input for theoretical modeling and atomistic simulations of PNIPAM in water. The attainment of this goal requires however a well understood phase diagram. Similar observations apply to a range of less explored water-soluble thermoresponsive polymers such as PVCL and PVME and their copolymers.

PNIPAM research as a whole made enormous progress<sup>[1–5]</sup> since the publication of the Heskins and Guillet<sup>[7]</sup> pioneering study of a PNIPAM phase diagram. Much of this progress is concerned with applications.<sup>[3]</sup> These PNIPAM applications harness a thermal response that is unanimously attributed to its phase diagram. Yet, the PNIPAM phase diagram itself awaits a definitive study and this subject remains a promising topic for future systematic research.

## Acknowledgements

C. Luap, E. Geissler, and L. Bureau critically read the manuscript and provided many helpful suggestions. We thank X. Zhang for drawing Schemes 1–3 and E. Korchagina for the photographs of PNIPAM solutions. F.M.W. gratefully acknowledges financial support from the Natural Sciences and Engineering Research Council of Canada, the World Premier International Research Center Initiative (WPI) MEXT, Japan, and the Finnish Academy of Science and Technology (TEKES), Finland. M.K. acknowledges support by the Swiss National Science Foundation through SNF grant 200021\_156106.

**How to cite:** *Angew. Chem. Int. Ed.* **2015**, *54*, 15342–15367  
*Angew. Chem.* **2015**, *127*, 2–15586

- [1] M. A. Cole, N. H. Voelcker, H. Thissen, H. J. Griesser, *Biomaterials* **2009**, *30*, 1827–1850.
- [2] E. S. Gil, S. M. Hudson, *Prog. Polym. Sci.* **2004**, *29*, 1173–1222.
- [3] V. Aseyev, H. Tenhu, F. M. Winnik, *Adv. Polym. Sci.* **2011**, *242*, 29–89.
- [4] R. Pelton, *Adv. Colloid Interface Sci.* **2000**, *85*, 1–33.
- [5] A. S. Hoffman, P. S. Stayton, *Prog. Polym. Sci.* **2007**, *32*, 922–932.
- [6] K. Nagase, J. Kobayashi, T. Okano, *J. R. Soc. Interface* **2009**, *6*, S293–S309.
- [7] M. Heskins, J. E. Guillet, *J. Macromol. Sci. Part A* **1968**, *2*, 1441–1455.
- [8] V. O. Aseyev, H. Tenhu, F. M. Winnik, *Adv. Polym. Sci.* **2006**, *196*, 1–85.

- [9] Z. M. O. Rzaev, S. Dincer, E. Piskin, *Prog. Polym. Sci.* **2007**, *32*, 534–595.
- [10] R. Koningsveld, W. H. Stockmayer, E. Nies, *Polymer Phase Diagrams: A Textbook*, Oxford University Press, Oxford, **2001**, pp. 79–86 and R. Koningsveld, W. H. Stockmayer, E. Nies, *Polymer Phase Diagrams: A Textbook*, Oxford University Press, Oxford, **2001**, pp. 137–160.
- [11] P. Sollich, *J. Phys. Condens. Matter* **2002**, *14*, R79–R117.
- [12] M. Kurata, *Thermodynamics of Polymer Solutions*, Gordon & Breach, London, **1982**, pp. 79–86.
- [13] K. Binder, M. Müller, P. Virnau, L. G. MacDowell, *Adv. Polym. Sci.* **2005**, *173*, 1–110.
- [14] M. Rubinstein, R. H. Colby, *Polymer Physics*, Oxford University Press, Oxford, **2003**.
- [15] P. G. Debenedetti, *Metastable Liquids: Concepts and Principles*, Princeton University Press, **1996**.
- [16] C. Boutris, E. G. Chatzi, C. Kiparissides, *Polymer* **1997**, *38*, 2567–2570.
- [17] T. Kawaguchi, Y. Kojima, M. Osa, T. Yoshizaki, *Polym. J.* **2008**, *40*, 455–459.
- [18] S. Fujishige, K. Kubota, I. Ando, *J. Phys. Chem.* **1989**, *93*, 3311–3313.
- [19] X. Zheng, Z. Tong, X. L. Xie, F. Zeng, *Polym. J.* **1998**, *30*, 284–288.
- [20] Z. Tong, F. Zeng, X. Zheng, *Macromolecules* **1999**, *32*, 4488–4490.
- [21] B. Ray, Y. Okamoto, M. Kamigaito, M. Sawamoto, K. Seno, S. Kanaoka, et al., *Polymer J.* **2005**, *37*, 234–237.
- [22] K. van Durme, G. V. Assche, B. V. Mele, *Macromolecules* **2004**, *37*, 9596–9605.
- [23] Y. Xia, N. A. D. Burke, H. D. H. Stover, *Macromolecules* **2006**, *39*, 2275–2283.
- [24] X. Zhou, J. Li, C. Wu, B. Zheng, *Macromol. Rapid Commun.* **2008**, *29*, 1363–1367.
- [25] K. Otake, H. Inomata, M. Konno, S. Saito, *Macromolecules* **1990**, *23*, 283–289.
- [26] R. Gomes de Azevedo, L. P. N. Rebelo, A. M. Ramos, J. Szydłowski, H. C. de Sousa, J. Klein, *Fluid Phase Equilib.* **2001**, *185*, 189–198.
- [27] L. P. N. Rebelo, Z. P. Visak, H. C. de Sousa, J. Szydłowski, R. G. de Azevedo, A. M. Ramos, et al., *Macromolecules* **2002**, *35*, 1887–1895.
- [28] R. Pamies, K. Zhu, A. L. Kjoniksen, B. Nystrom, *Polym. Bull.* **2009**, *62*, 487–502.
- [29] F. Afroze, E. Nies, H. Berghmans, *J. Mol. Struct.* **2000**, *554*, 55–68.
- [30] F. Shi, Z. Han, J. Li, B. Zheng, C. Wu, *Macromolecules* **2011**, *44*, 686–689.
- [31] M. Philipp, R. Aleksandrova, U. Müller, M. Ostermeyer, R. Sanctuary, P. Müller-Buschbaum, et al., *Soft Matter* **2014**, *10*, 7297–7305.
- [32] X. Qiu, T. Koga, F. Tanaka, F. Winnik, *Sci. China Chem.* **2013**, *56*, 56–64.
- [33] S. Habaue, Y. Isobe, Y. Okamoto, *Tetrahedron* **2002**, *58*, 8205–8209.
- [34] Y. Katsumoto, N. Kubosaki, *Macromolecules* **2008**, *41*, 5955–5956.
- [35] K. Nishi, T. Hiroi, K. Hashimoto, K. Fujii, Y. S. Han, T. H. Kim, et al., *Macromolecules* **2013**, *46*, 6225–6232.
- [36] S. Nakano, T. Ogiso, R. Kita, N. Shinyashiki, S. Yagihara, M. Yoneyama, et al., *J. Chem. Phys.* **2011**, *135*, 114903.
- [37] T. Hirano, H. Miki, M. Seno, T. Sato, *Polymer* **2005**, *46*, 5501–5505.
- [38] K. Chan, R. Pelton, J. Zhang, *Langmuir* **1999**, *15*, 4018–4020.
- [39] J. E. Chung, M. Yokoyama, K. Suzuki, T. Aoyagi, Y. Sakurai, T. Okano, *Colloids Surf. B* **1997**, *9*, 37–48.
- [40] J. E. Chung, M. Yokoyama, T. Aoyagi, Y. Sakurai, T. Okano, *J. Controlled Release* **1998**, *53*, 119–130.
- [41] S. Furyk, Y. Zhang, D. Ortiz-Acosta, P. S. Cremer, D. E. Bergbreiter, *J. Polym. Sci. Part A* **2006**, *44*, 1492–1501.
- [42] Z. Liu, Q. Liao, D. Yang, Y. Gao, X. Luo, Z. Lei, et al., *Des. Monomers Polym.* **2013**, *16*, 465–474.
- [43] T. Kawaguchi, Y. Kojima, M. Osa, T. Yoshizaki, *Polym. J.* **2008**, *40*, 528–533.
- [44] A. V. Gorelov, A. D. Chesne, K. A. Dawson, *Phys. A* **1997**, *240*, 443–452.
- [45] C. Wu, X. Wang, *Phys. Rev. Lett.* **1998**, *80*, 4092–4094.
- [46] V. Aseyev, S. Hietala, A. Laukkanen, M. Nuopponen, O. Confortini, F. E. D. Prez, et al., *Polymer* **2005**, *46*, 7118–7131.
- [47] H. Cheng, L. Shen, C. Wu, *Macromolecules* **2006**, *39*, 2325–2329.
- [48] Y. Maeda, T. Higuchi, I. Ikeda, *Langmuir* **2000**, *16*, 7503–7509.
- [49] C. Balu, M. Delsanti, P. Guenoun, *Langmuir* **2007**, *23*, 2404–2407.
- [50] A. Meier-Koll, V. Pipich, P. Busch, C. M. Papadakis, P. Müller-Buschbaum, *Langmuir* **2012**, *28*, 8791–8798.
- [51] P. Kujawa, F. M. Winnik, *Macromolecules* **2001**, *34*, 4130–4135.
- [52] P. Kujawa, V. Aseyev, H. Tenhu, F. M. Winnik, *Macromolecules* **2006**, *39*, 7686–7693.
- [53] H. Tanaka, *Macromolecules* **1992**, *25*, 6377–6380.
- [54] S. Bolisetty, C. Schneider, F. Polzer, M. Ballauff, W. Li, A. Zhang, et al., *Macromolecules* **2009**, *42*, 7122–7128.
- [55] R. Koningsveld, A. J. Staverman, *J. Polym. Sci. A-2* **1968**, *6*, 325–347.
- [56] I. H. Park, Q. W. Wang, B. Chu, *Macromolecules* **1987**, *20*, 1965–1975.
- [57] H. Tanaka, *Phys. Rev. Lett.* **1993**, *71*, 3158.
- [58] A. Y. Grosberg, D. V. Kuznetsov, *Macromolecules* **1993**, *26*, 4249–4251.
- [59] E. D. Siggia, *Phys. Rev. A* **1979**, *20*, 595–605.
- [60] “Kinetics of Flocculation”: J. T. G. Overbeek, *Colloid Science, Vol 1* (Ed.: H. R. Kruyt), Elsevier, Amsterdam, **1952**, p. 278.
- [61] B. Chu, Q. Ying, A. Y. Grosberg, *Macromolecules* **1995**, *28*, 180–189.
- [62] J. Chuang, A. Y. Grosberg, T. Tanaka, *J. Chem. Phys.* **2000**, *112*, 6434–6442.
- [63] A. Y. Grosberg, S. K. Nechaev, E. I. Shakhnovich, *J. Phys.* **1988**, *49*, 2095–2100.
- [64] E. Jarkova, A. Johner, E. A. Maresov, A. N. Semenov, *Eur. Phys. J. E* **2006**, *21*, 371–386.
- [65] G. Karlström, *J. Phys. Chem.* **1985**, *89*, 4962–4964.
- [66] Y. Okada, F. Tanaka, *Macromolecules* **2005**, *38*, 4465–4471.
- [67] A. Y. Grosberg, *Biophys.* **1984**, *29*, 621–626.
- [68] H. Tanaka, *J. Chem. Phys.* **1994**, *100*, 5323.
- [69] A. Bhattacharya, S. D. Mahanti, A. Chakrabarti, *Phys. Rev. Lett.* **1998**, *80*, 333–336.
- [70] H. Liu, A. Bhattacharya, A. Chakrabarti, *J. Chem. Phys.* **1999**, *111*, 11183.
- [71] O. Peleg, M. Kröger, I. Hecht, Y. Rabin, *EPL* **2007**, *77*, 58007.
- [72] E. A. Maresov, A. N. Semenov, *Macromolecules* **2008**, *41*, 9439–9457.
- [73] V. V. Vasilevskaya, P. G. Khalatur, A. R. Khokhlov, *Macromolecules* **2003**, *36*, 10103–10111.
- [74] A. S. Ushakova, E. N. Govorunand, A. R. Khokhlov, *J. Phys. Condens. Matter* **2006**, *18*, 915–930.
- [75] K. Dušek, *Collect. Czech. Chem. Commun.* **1969**, *34*, 3309.
- [76] K. Šolc, K. Dušek, R. Koningsveld, H. Berghmans, *Collect. Czech. Chem. Commun.* **1995**, *160*, 1661.
- [77] P. G. de Gennes, *C. R. Acad. Sci.* **1991**, *313*, 1117–1122.
- [78] V. A. Baulin, A. Halperin, *Macromolecules* **2002**, *35*, 6432–6438.
- [79] A. Matsuyama, F. Tanaka, *Phys. Rev. Lett.* **1990**, *65*, 341.
- [80] B. A. Veytsman, *J. Phys. Chem.* **1990**, *94*, 8499–8500.

- [81] S. Bekiranov, R. Bruinsma, P. Pincus, *Phys. Rev. E* **1997**, *55*, 577–585.
- [82] E. E. Dormidontova, *Macromolecules* **2002**, *35*, 987–1001.
- [83] M. Wagner, F. Brochard-Wyart, H. Hervet, P. G. de Gennes, *Colloids Polym. Sci.* **1993**, *271*, 621.
- [84] P. W. Zhu, D. H. Napper, *J. Colloid Interface Sci.* **1994**, *164*, 489–494.
- [85] R. Plummer, D. J. T. Hill, A. K. Whittaker, *Macromolecules* **2006**, *39*, 8379–8388.
- [86] V. A. Baulin, E. B. Zhulina, A. Halperin, *J. Chem. Phys.* **2003**, *119*, 10977–10988.
- [87] V. A. Baulin, A. Halperin, *Macromol. Theory Simul.* **2003**, *12*, 549–559.
- [88] A. Halperin, M. Kröger, *Macromolecules* **2011**, *44*, 6986–7005.
- [89] H. Yim, M. S. Kent, S. Satija, S. Mendez, S. S. Balamurugan, S. Balamurugan, et al., *Phys. Rev. E* **2005**, *72*, 051801.
- [90] G. Moad, E. Rizzardo, S. H. Thang, *Aust. J. Chem.* **2005**, *58*, 379–410.
- [91] C. Schilli, M. G. Lanzendörfer, A. H. E. Müller, *Macromolecules* **2002**, *35*, 6819.
- [92] B. Ray, Y. Isobe, K. Morioka, S. Habaue, Y. Okamoto, M. Kamigaito, et al., *Macromolecules* **2003**, *36*, 543–545.
- [93] T. Biadatti, P. Corpart, D. Charmot, S. Z. Zard, D. Michelet, *Method for block polymer synthesis by controlled radical polymerisation*, Patent WO1998058974A1, 1998.
- [94] E. Read, A. Guinaudeau, D. J. Wilson, A. Cadix, F. Violleau, M. Destarac, *Polym. Chem.* **2014**, *5*, 2202–2207.
- [95] J. Gao, B. J. Frisken, *Langmuir* **2003**, *19*, 5212–5216.
- [96] O. L. J. Virtanen, H. M. Ala-Mutka, W. Richtering, *Macromol. Chem. Phys.* **2015**, *216*, 1431–1440.
- [97] X. Wang, X. Qiu, C. Wu, *Macromolecules* **1998**, *31*, 2972–2976.
- [98] S. Fujishige, *Polym. J.* **1987**, *19*, 297–300.
- [99] R. Freitag, F. Garret-Flaudy, *Langmuir* **2002**, *18*, 3434–3440.
- [100] K. Nagahama, H. Inomata, S. Saito, *Fluid Phase Equilib.* **1994**, *96*, 203–214.
- [101] H. Inomata, Y. Yagi, K. Otake, M. Konno, S. Saito, *Macromolecules* **1989**, *22*, 3494–3495.
- [102] “Development of models for large molecules and electrolytes in solution for process engineering”: J. Walter, S. Deublein, J. Vrabec, H. Hasse in *High Performance Computing in Science and Engineering '09 Transactions of the High Performance Computing Center* (Ed.: W. E. Nagel), Stuttgart (HLRS) 2009, **2010**, pp. 165–172.
- [103] D. Prada-Gracia, R. Shevchuk, F. Rao, *J. Chem. Phys.* **2013**, *139*, 084501.
- [104] A. Halperin, M. Kröger, *Biomaterials* **2012**, *33*, 4975–4987.
- [105] F. Zeng, Z. Tong, X. Z. Yang, *Eur. Polym. J.* **1997**, *33*, 1553–1556.
- [106] A. Milewska, J. Szydłowski, L. P. N. Rebelo, *J. Polym. Sci. Part B* **2003**, *41*, 1219–1233.
- [107] K. Poschlade, S. Enders, *J. Chem. Thermodyn.* **2011**, *43*, 262–269.
- [108] C. Hashimoto, A. Nagamoto, T. Maruyama, N. Kariyama, Y. Iriya, A. Ikehata, et al., *Macromolecules* **2013**, *46*, 1041–1053.

Received: July 19, 2015

Published online: November 27, 2015